



THESIS APPROVAL
GRADUATE SCHOOL, KASETSART UNIVERSITY

Master of Engineering (Chemical Engineering)

DEGREE

Chemical Engineering

Chemical Engineering

FIELD

DEPARTMENT

TITLE: Methane Cracking Over Nickel Loaded On Bimodal Porous Silica Supports

NAME: Mr. Jakkraphun Kitmanacharounpong

THIS THESIS HAS BEEN ACCEPTED BY

THESIS ADVISOR

(Associate Professor Metta Chareonpanich, D.Eng.)

THESIS CO-ADVISOR

(Mr. Thongthai Witoon, D.Eng.)

DEPARTMENT HEAD

(Associate Professor Apinya Duangchan, Ph.D.)

APPROVED BY THE GRADUATE SCHOOL ON

DEAN

(Associate Professor Gunjana Theeragool, D.Agr.)

THESIS

METHANE CRACKING OVER NICKEL LOADED ON BIMODAL
POROUS SILICA SUPPORTS

The seal of Kasetsart University is a large, light green circular emblem. It features a central figure, likely a deity or royal figure, surrounded by a decorative border. The words "KASETSART UNIVERSITY" are written in a semi-circle at the top, and the year "1943" is at the bottom. Two small floral motifs are positioned on the left and right sides of the seal.

JAKKGRAPHUN KITMANACHAROUNPONG

A Thesis Submitted in Partial Fulfillment of
the Requirements for the Degree of
Master of Engineering (Chemical Engineering)
Graduate School, Kasetsart University
2012

Jakkraphun Kitmanacharounpong 2012: Methane Cracking Over Nickel Loaded on Bimodal Porous Silica Supports. Master of Engineering (Chemical Engineering), Major Field: Chemical Engineering, Department of Chemical Engineering. Thesis Advisor: Associate Professor Metta Chareonpanich, D.Eng. 89 pages.

In this research, methane cracking reaction (MCR) was studied over nickel loaded on bimodal porous silica supports. The supports used in this study were bimodal porous silica (BS) consisting mesopore and macropore of two different pore sizes (BS-1 and BS-2 for prepared by using pH value of 3 and 5, respectively). These supports were synthesized by a simple sol-gel method and chitosan template was used to create the macropore structure in the mesoporous silica frameworks. After that, 5 wt.% nickel was loaded onto bimodal porous silica supports via incipient-wetness impregnation method. The monomodal porous silica supports (MS-1 and MS-2 for prepared by using pH value of 3 and 5, respectively) were also synthesized for comparison. The obtained catalysts were analyzed by using N₂-sorption, X-ray diffraction (XRD) and Scanning Electron Microscopy (SEM). The performances of MCR of these catalysts were tested under atmospheric pressure and the operating temperatures of 500, 550, 600 and 650°C using methane flow rate of 20 ml/min. The outlet gases were analyzed by using gas chromatography while the used catalysts and solid carbon products were examined by using thermogravimetric analysis (TGA). The results showed that CH₄ conversion and H₂ yield of Ni/BS-1 and Ni/BS-2 were higher than those of Ni/MS-1 and Ni/MS-2. It could be explained that the interconnected, relatively large pore of monomodal porous silica supports would not be appropriate for methane cracking reaction, leading to the lower CH₄ conversion and H₂ yield. CH₄ conversion and H₂ yield from MCR did not depend on operating temperatures for Ni/MS as the negative activation energies were obtained while Ni/BS obtained, which provide the positive activation energy, were depended on operating temperature.

Student's signature

Thesis Advisor's signature

ACKNOWLEDGEMENTS

I would like to take this opportunity to acknowledge the people who have helped to make this work possible. My sincere gratitude first goes to my thesis advisor Associate Professor Metta Chareonpanich, for her consistent and thoughtful advice, continuous encouragement and help during the course of this work. Moreover, I am grateful to my graduate committees, Doctor Thongthai Witoon for their kindly giving the time to advice, revise and approve my thesis.

I am grateful to my fellow graduate students at Department of Chemical Engineering, Kasetsart University for assisting me my research and offering valuable suggestion.

The financial supports by the Center of Nanotechnology Kasetsart University and the Graduate School at Kasetsart University, Kasetsart University Research and Development Institute (KURDI) and the National Excellence Center for Petroleum, Petrochemicals and Advanced Materials are acknowledged.

Finally, I would like to thank my family for their love, support, encouragement, and their understanding during the whole period of my education. My family has been my greatest source of strength and inspiration. My gratefulness devotes to my family who wholeheartedly support me away.

Jakkraphun Kitmanacharounpong

April 2012

TABLE OF CONTENTS

	Page
TABLE OF CONTENTS	i
LIST OF TABLES	ii
LIST OF FIGURES	iii
INTRODUCTION	1
OBJECTIVES	3
LITERATURE REVIEW	4
MATERIALS AND METHODS	28
RESULTS AND DISCUSSION	40
CONCLUSION	68
LITERATURE CITED	69
APPENDICES	75
Appendix A Qualitative and quantitative results from gas chromatography	76
Appendix B Conversion and selectivity results	80
Appendix C Diameter of crystallite nickel oxide calculation	83
Appendix D Activation energy calculation	85
CURRICULUM VITAE	89

LIST OF TABLES

Table	Page
1 Details of conversions obtained in the present study with different supports at 998 K and 2700 h ⁻¹ GHSV	21
2 Synthesis conditions for monomodal porous silica supports and bimodal meso-macroporous silica supports	32
3 Physical properties of loaded and unloaded monomodal porous silica supports	45
4 Activation energy of nickel loaded on monomodal and bimodal porous silica supports	67
 Appendix Table	
A1 Equation of calibration curves for standard gas	79
B1 Example of conversion and yield of methane cracking reaction over Ni/BS-2 catalyst	82
D1 Summarized κ and operating temperature	87
D2 Summarized activation energies of nickel supported on monomodal and bimodal porous silica supports	88

LIST OF FIGURES

Figure		Page
1	Schematic of the classical mechanism of carbon filament formation	5
2	Particle detachment and formation of (a) solid filament and (b) hollow filament	6
3	SEM images of 5 wt% Ni/ α -Al ₂ O ₃ catalyst after (a) 14 h reaction at 650°C, (b) 13 h reaction at 600°C, (c) 8 h reaction at 550°C and (d) 16 h reaction at 500°C	8
4	Cross sections of conical graphite layers excreted in a direction perpendicular to the metal/filament interface (a) without slippage, (b) with slippage	9
5	Adsorption from solution containing [Pt(NH ₃) ₄] ²⁺ onto silica gel and γ -alumina as a function of pH. Room temperature. O, silica gel; γ -alumina	10
6	SEM image of Ni/SBA-15 with different preparation method: (a) incipient wetness impregnation (IWI), (b) grafting with silane coupling agents (SA) and (c) in situ reduction (IR)	11
7	Hydrogen evolution in reactor tests at 700°C with the Ni/TiO ₂ and Ni-Cu/TiO ₂ catalysts prepared by impregnation and fusion method	12
8	Methane conversion over different nickel content supported on SiO ₂ catalysts at 600°C	13
9	Over view of sol-gel process	15
10	Polymerization behavior of silica: (A) in acid solution or a presence of flocculating salts, particles aggregate into three-dimensional networks and form gels; (B) in basic solution particles in sol grow in size with decrease in numbers	17

LIST OF FIGURES (Continued)

Figure		Page
11	Methane conversion over Ni/SiO ₂ at 600°C (■), 550°C (●) and 500°C (▲)	18
12	Hydrogen evolution with the fusion catalysts calcined at different temperatures (a) Ni–Ti catalysts and (b) Ni–Cu–Ti catalysts	20
13	Methane conversion over Ni catalysts supported on different supports at 500°C	22
14	H ₂ -TPR patterns of Co-SBA-15 and SBA-15 with impregnated cobalt	23
15	Formation scheme of the bimodal pore support	24
16	Pore size distribution of Q-50 and the bimodal porous supports: (A) silicaQ-50 (B) bimodal porous silica support (C) Zr/bimodal porous support	24
17	SEM images (a) and TEM images (b) of mixed-phase bimodal mesoporous silicas	26
18	TEM image of meso-macroporous silica with adjusting pH (a) pH = 3 and (b) pH = 5	27
19	Schematic diagram of sodium silicate synthesis process	30
20	Schematic diagram of bimodal porous silica synthesis	32
21	Catalytic reaction testing unit: (a) a feed flow measuring and controlling system, (b) a furnace-equipped stainless steel tube reactor and (c) a sampling system	35
22	Mass flow controller(Aalborg GFC thermal mass flow controller)	36
23	The reactor of methane cracking reaction equipped with the electric heater (Carbolite tube furnace)	37
24	Schematic setup of the stage of methane cracking reaction reactor	37
25	Shimadzu gas chromatograph (GC-2014) equipped with thermal conductivity detector (TCD) and chromatopac data processor	38

LIST OF FIGURES (Continued)

Figure		Page
26	Isotherm of porous silica supports including (a) monomodal and (b) bimodal porous silica supports and nickel supported on porous silica supports including (c) monomodal and (d) bimodal porous silica supports	42
27	Pore size distributions of (a) MS-1, (b) MS-2, (c) BS-1 and (d) BS-2	43
28	Pore size distributions of (a) Ni/MS-1, (b) Ni/MS-2, (c) Ni/BS-1 and (d) Ni/BS-2	44
29	XRD patterns of nickel supported on monomodal and bimodal porous silica supports	46
30	Catalytic activities of Ni/MS-1 catalyst (a) CH ₄ conversion and (b) H ₂ yield	48
31	Catalytic activities of Ni/MS-2 catalyst (a) CH ₄ conversion and (b) H ₂ yield	49
32	Catalytic activities of Ni/BS-1 catalyst (a) CH ₄ conversion and (b) H ₂ yield	51
33	Catalytic activities of Ni/BS-2 catalyst (a) CH ₄ conversion and (b) H ₂ yield	52
34	(a) TGA and (b) DTA of Ni/MS-1 catalyst	54
35	(a) TGA and (b) DTA of Ni/MS-2 catalyst	55
36	(a) TGA and (b) DTA of Ni/BS-1 catalyst	57
37	(a) TGA and (b) DTA of Ni/BS-2 catalyst	58
38	SEM images of Ni/MS-1 performed methane cracking reaction at (a) 650°C, (b) 600°C, (c) 550°C and (d) 500°C	60
39	SEM images of Ni/MS-2 performed methane cracking reaction at (a) 650°C, (b) 600°C, (c) 550°C and (d) 500°C	61

LIST OF FIGURES (Continued)

Figure		Page
40	SEM images of Ni/BS-1 performed methane cracking reaction at (a) 650°C, (b) 600°C, (c) 550°C and (d) 500°C	63
41	SEM images of Ni/BS-2 performed methane cracking reaction at (a) 650°C, (b) 600°C, (c) 550°C and (d) 500°C	64
42	Arrhenius plot of nickel supported on (a) monomodal and (b) bimodal porous silica supports	66
Appendix Figure		Page
A1	Schematic diagram of gas chromatograph	77
A2	Chromatogram of standard gases for CO, CH ₄ and CO ₂	78
D1	Arrhenius's plot of Ni/BS-2 catalyst	88

METHANE CRACKING OVER NICKEL LOADED ON BIMODAL POROUS SILICA SUPPORTS

INTRODUCTION

In present, there are many interests of hydrogen as the clean energy because of its clean combustion product of water. Methane is a preferred source of hydrogen because it gives a high ratio of hydrogen to carbon (Poirier and Sapundzhiev, 1997). There are many processes to produce hydrogen from methane reactant such as methane steam reforming (MSR), partial oxidation of methane (POM) and methane cracking reaction (Choudhary *et al.*, 2001). Methane cracking reaction can perform in the lower temperature when compared to the MSR and POM, therefore, many attempts have been focused on methane cracking reaction (Aiello *et al.*, 2000; Alstrup, 1988).

In the case of metal catalysts used for methane cracking reaction, the transition metals are widely used especially Ni, Fe and Co (Alstrup, 1988) which can produce hydrogen (Villacampa *et al.*, 2003), carbonaceous filament (Niu and Fang, 2007), carbon nanotubes (Ichioka *et al.*, 2007) and carbon fibers (Venugopal *et al.*, 2007). Among these catalysts, nickel is often used as an active metal for methane cracking reaction than other reactions due to its low cost and high catalytic activity to produce hydrogen and carbonaceous filaments (Pompeo *et al.*, 2009).

Silica (SiO_2) is selected as the supports for methane cracking reaction due to its low metal-support interaction and large pore (Ermokova *et al.*, 2000). However, the carbonaceous filaments produced from the decomposition of methane are the major problem for this process because they will block the pores of catalyst supports, leading to rapid deactivation of catalysts. Therefore, bimodal porous supports containing two different pore sizes are synthesized to overcome the pore blockage of carbonaceous filament. The bimodal porous catalysts can be simply prepared by impregnating the metal oxide sols such as SiO_2 , ZrO_2 , Al_2O_3 and TiO_2 into silica gel

(Shinoda *et al.*, 2004). The other bimodal porous catalysts can also be synthesized by using the sol-gel method with specific templates such as chitosan (Witoon *et al.*, 2008), hyperbranched polyester (H20M) (Zhao *et al.*, 2006) and cetyltrimethyl ammonium bromide (CTMABr) (Morales *et al.*, 2005), and then adjusted the pH of mixture to create the extra pore in their structures. The other way to synthesize bimodal porous silica is the mixing template method using two different types of template such as CTAB and Pluronic P123 (Jullphan *et al.* 2009) to synthesize the mixed phase of SBA-15 and SBA-3-like porous silica. It should be mentioned that the bimodal porous materials could provide the larger pores and decrease the carbonaceous filament blockage, leading to increase the methane cracking reaction catalytic activity.

In this research, the bimodal porous silica supports were synthesized to overcome the pore blockage of carbonaceous filament produced from methane cracking reaction. The macroporous structure was created in the silica frameworks by using natural chitosan template. Then, nickel precursor of 5 wt.% Ni was loaded onto porous silica supports. The physical properties of nickel-based catalysts were analyzed via N₂-sorption, X-ray diffraction (XRD) and Scanning electron microscopy (SEM) technique. Nickel-based catalysts were tested for performance in methane cracking reaction under the operating temperatures of 500, 550, 600 and 650°C. Moreover, in order to investigate the effect of macroporosity and pore blockage, nickel supported on monomodal porous silica supports was also tested.

1943

OBJECTIVES

1. To synthesize bimodal meso-macro porous silica supports in the pore ranges meso-macropores.
2. To study the effect of bimodal meso-macro porous silica supports on performances of methane cracking reaction catalytic.
3. To study the effect of operating temperature on methane cracking reaction over monomodal and bimodal porous silica supports.

Benefit

Know how of application of bimodal meso-macro porous silica supports for methane cracking reaction.

LITERATURE REVIEW

Methane cracking reaction is the well-known reaction to produce hydrogen and carbonaceous filament. One of the appropriate metal catalyst for methane cracking reaction is nickel (Ni), this is due to its low cost and high activity for decomposition of methane (Naito, 2000). In the case of support methane cracking catalysts, the frequently used supports are silica (SiO₂), titania (TiO₂) and alumina (Al₂O₃). However, the nickel-based catalysts showed low stability due to the pore blockage from carbonaceous filament products (Zhang and Amiridis, 1998). Bimodal porous silica supports consisting two difference pore sizes can possibly solve the pore blockage problem. This research focuses on the study of carbonaceous filament production and consequently improves the methane cracking reaction. The background informations including methane cracking reaction, the metal catalysts and supported catalysts for methane cracking reaction are reviewed as the details shown below.

1. Methane cracking reaction

The hydrogen was synthesized from various well-known reaction such as partial oxidation of methane (POM), steam reforming of methane (SRM) and methane cracking reaction. Among these reactions, methane cracking reaction was the most interesting reaction because the lowest temperature was required. According to its low enthalpy, the operating temperature was slightly lower than those of POM (-36 KJ/mol) (Deutschmann and Schmidt, 1998) and SRM (206 KJ/mol) (Mohamed, 2011). The reaction temperature of methane cracking reaction had been reported to be below as 500°C. Methane cracking reaction was shown below:



The methane cracking reaction is started with the decomposition of methane on the metal surface (at the gas side) to form carbon and hydrogen products. Then,

carbon dissolved in the metal particle, diffused through the particle and precipitated on the metal-support interface, as shown in Figure 1 (Snoeck *et al.*, 1997).

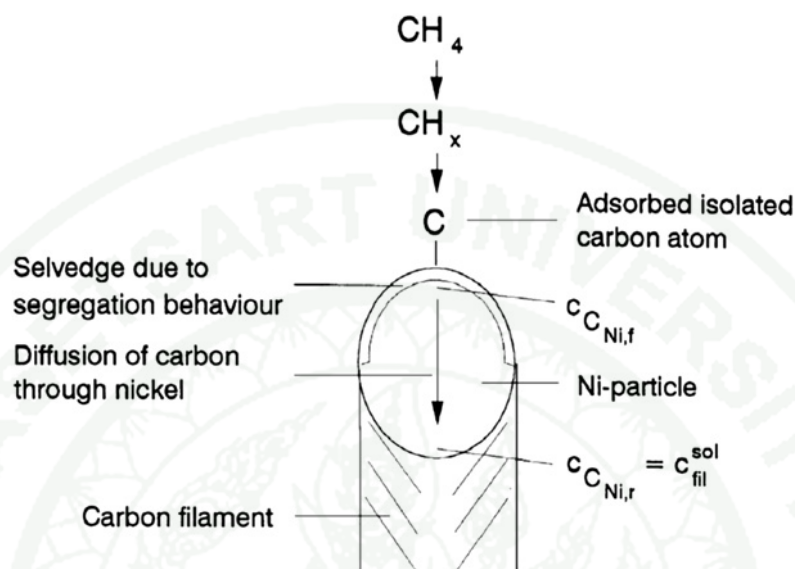


Figure 1 Schematic of the classical mechanism of carbon filament formation.

Source: Snoeck *et al.* (1997)

The carbonaceous filament was produced from methane cracking reaction. Kock *et al.* (1985) proposed the carbonaceous filaments formation over 50 wt.% Ni/SiO₂. The nucleation was the first step of carbonaceous filament growth which started with the carburization of deposited carbon to form nickel carbide. Then, nickel carbide was decomposed and started the nucleation of graphite. After that, graphite was precipitated at the nickel-support interface and detach nickel particle from support.

The carbonaceous filaments would be solid or hollow were depended on the operating temperatures. At low temperature, the carbon diffusion rate through nickel particle was slower than the nucleation and precipitation rate. Moreover, the nucleation was more uniform at the metal-support interface. Therefore, the solid carbonaceous filaments would be formed, as shown in Figure 2a. On the contrary, at high temperature, the distortion of nickel particles had been observed. Furthermore,

the nucleation and precipitation occurred at gas-metal interface and their rates were higher than those of diffusion rate. As a result, the hollow carbonaceous filament would be occurred, as shown in Figure 2b (Snoeck *et al.*, 1997).

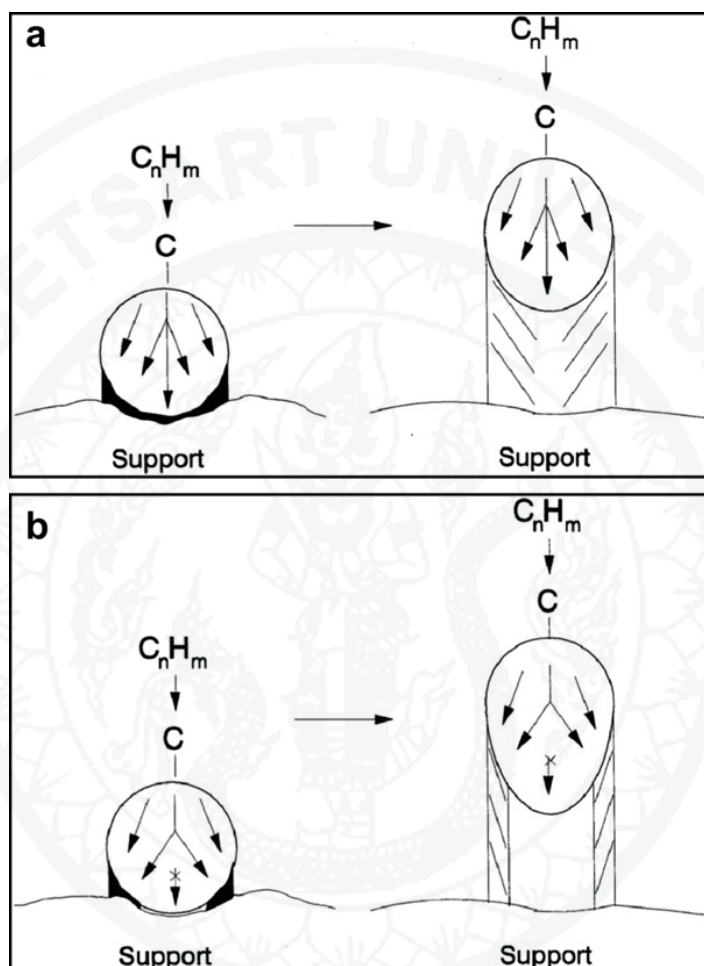


Figure 2 Particle detachment and formation of (a) solid filament and (b) hollow filament.

Source: Snoeck *et al.* (1997)

Zhang and Amiridis (1998) used Ni/Al₂O₃ catalyst to investigate the appropriate operating temperatures for methane cracking. They found that the optimum temperatures were in the range of 500-552°C. Moreover, at 552°C the maximum CH₄ conversion was observed due to the fact that the rate of carbon

deposition on nickel particle was in equilibrium with the rate of surface carbon migration and diffusion through nickel particle. For the operating temperature below 500°C, the rate of migration and diffusion were higher than those of the rate of carbon deposition, leading to the carbonaceous filament grew at the metal-support interface. Then, carbonaceous filament detached nickel particles out of the support. After the detachment, nickel particle was now supported by carbon filament and the concentration of carbon at the metal-filament interface drop to the saturation concentration of filamentous carbon. Nickel particle now acted as a heat sink (Baker *et al.*, 1972). As a result, the carbonaceous filament growth rate was higher than those of high operating temperature. On the other hand, at the temperature beyond 552°C, the rate of carbon deposition was higher than those of surface carbon migration and diffusion. Therefore, carbon could grow on both sides of nickel particle and encapsulate the nickel particle, leading to lower methane conversion (Zang and Amiridis, 1998).

The diameter of carbonaceous filaments was also affected from the operating temperature. Rahman *et al.* (2006) studied the influence of temperature to the diameter of carbonaceous filaments. For temperatures between 500 and 650°C, the diameter of carbonaceous filaments was decreased with increasing temperature, as shown in Figure 3.

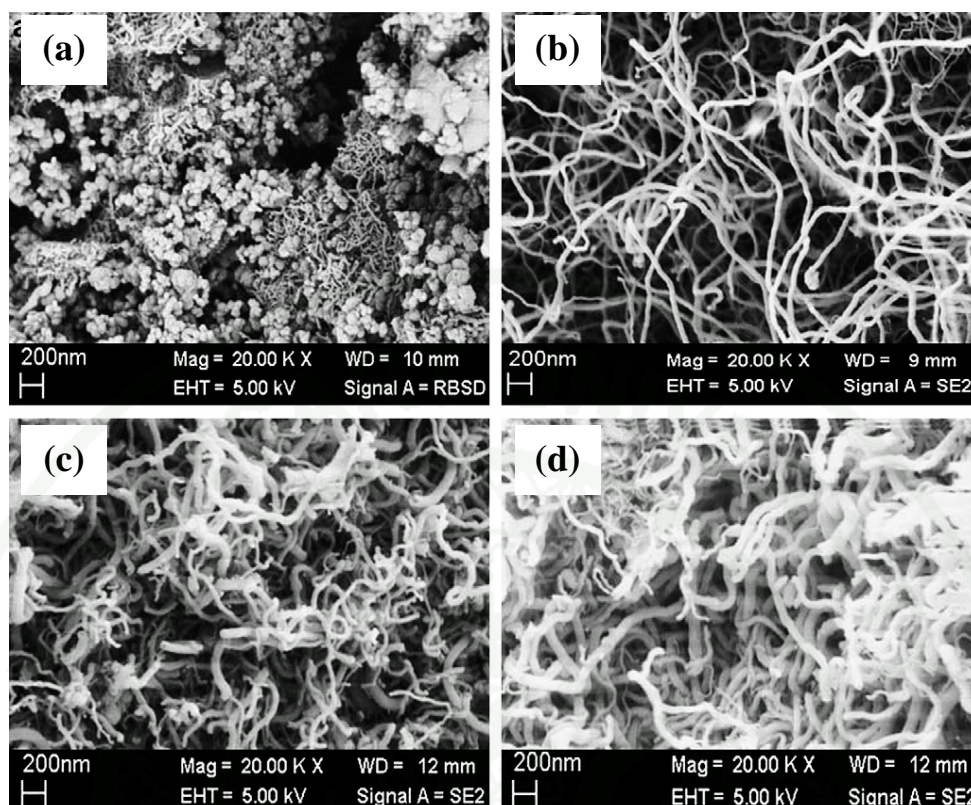


Figure 3 SEM images of 5 wt% Ni/ α -Al₂O₃ catalyst after (a) 14 h reaction at 650°C, (b) 13 h reaction at 600°C, (c) 8 h reaction at 550°C and (d) 16 h reaction at 500°C.

Source: Rahman *et al.* (2006)

Moreover, the conical shape of carbonaceous filament had been reported by Boellard *et al.* (1985). The conical shape of carbonaceous filament was also called fish-bone-like structures resembled from coke layers. The carbon species were excreted from the metal particle perpendicular to the metal-filament interface and deposited upon one another in a conical form, as shown in Figure 4(a). The perimeter of conical carbonaceous filament increased along with the formation leading to the expansion of carbonaceous filament. However, it was proposed that the diameter of conical carbonaceous filament was constant over very long distance which could not support the increasing of perimeter. Therefore, the other mechanism containing the concept of slippage had been proposed instead. The excreted coke layers pushed

metal particles upward along the direction of the filament axis, so that the filament diameter remained constant, as shown in Figure 4(b).

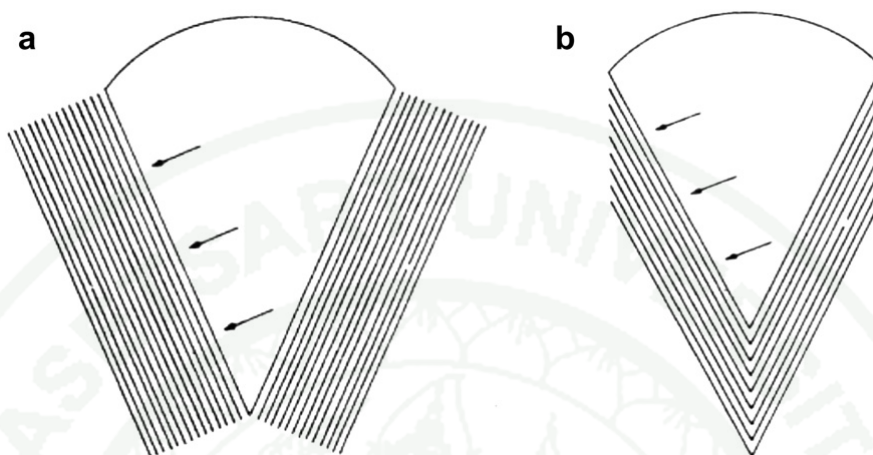


Figure 4 Cross sections of conical graphite layers excreted in a direction perpendicular to the metal/filament interface (a) without slippage, (b) with slippage.

Source: Boellaard *et al.* (1985)

2. Metal catalysts for methane cracking reaction

Iron catalyst group had been reported to be appropriate to methane cracking reaction (Avdeeva *et al.*, 2002). According to the best selection of metal catalysts, the basic metal loading methods and metal catalysts for metal-support reaction are described as shown below:

2.1. Incipient wetness impregnation method

An incipient wetness impregnation method is usually used to prepare the catalyst by adding metal salt solution into the pores of support. The volume of metal solution is slightly larger than those of the volume of support pores ('wet' impregnation). The incipient wetness impregnation method is started with a sufficient

concentration of metal is dissolved by water. Then, the metal solution was slowly added to powdered support stirred vigorously to obtain the distributed homogeneous solution. Moreover, the powdered catalysts would be obtained after the solution was aged, then dried and calcined. The adsorption effect in wet impregnation method could describe in terms of pH solution. At low pH, the adsorption of metal on the support was very slow while at high pH, limit at 9, the metal was highly adsorbed on the support, as shown in Figure 5 (Moulijn *et al.*, 1993).

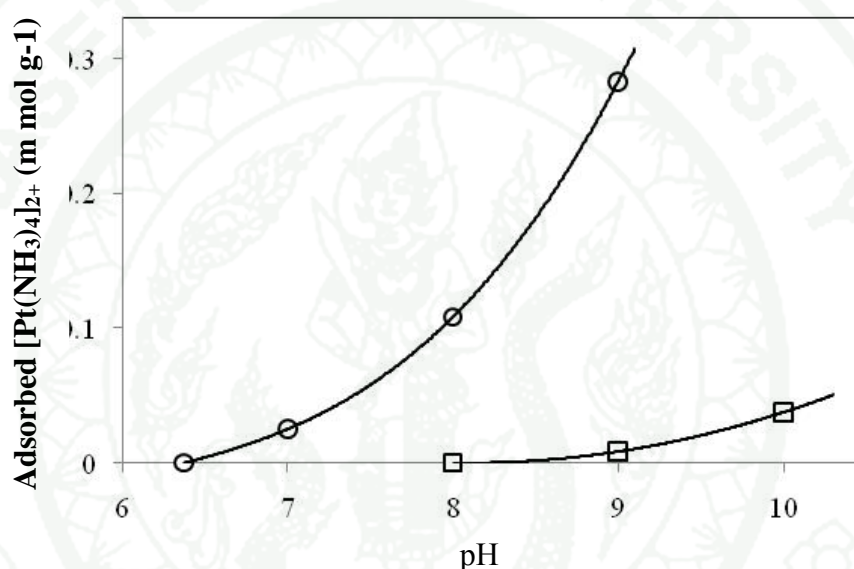


Figure 5 Adsorption from solution containing $[\text{Pt}(\text{NH}_3)_4]^{2+}$ onto silica gel and γ -alumina as a function of pH. Room temperature. O, silica gel; γ -alumina.

Source: Moulijn *et al.* (1993)

Zhang *et al.* (2008) studied the effect of metal loading method onto methane cracking reaction performance. They used incipient wetness impregnation method (IWI), grafting with silane coupling agents (SA) and in situ reduction (IR) to prepare the nickel-based catalysts, as shown in Figure 6. In the case of IWI, carbon nanotubes (CNTs) grew on the outer surface and blocked the pores of supports, leading to the formation of abundant CNTs with very large inner diameter. For SA method, metal catalysts were highly dispersed, causing the few CNTs growth on the outer surface

with a uniform inner diameter of smaller than the pore sizes of SBA-15. However, there was more carbon deposited within the pore channels. For IR method, homogeneously coated on the inner pore wall surface was occurred in the catalyst. However, the CNTs were not observed on the outer surface of SBA-15, while the ordered carbon mesopore structures had been obtained.

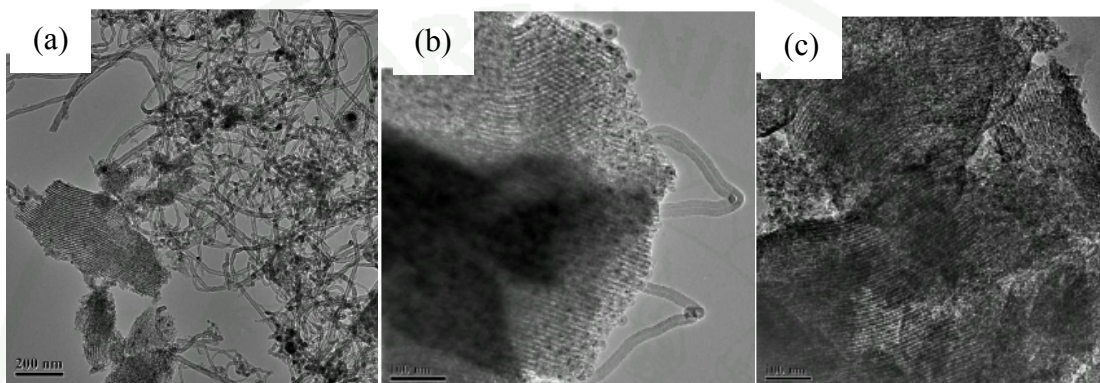


Figure 6 SEM image of Ni/SBA-15 with different preparation method: (a) incipient wetness impregnation (IWI), (b) grafting with silane coupling agents (SA) and (c) in situ reduction (IR).

Source: Zhang *et al.* (2008)

Lázaro *et al.* (2008) also studied the effect of catalyst preparation method on the catalytic cracking of methane. They loaded nickel onto TiO_2 by using IWI and fusion methods. They found that IWI method exhibited the lower stability of catalysts when compare to that of the fusion method, as shown in Figure 7.

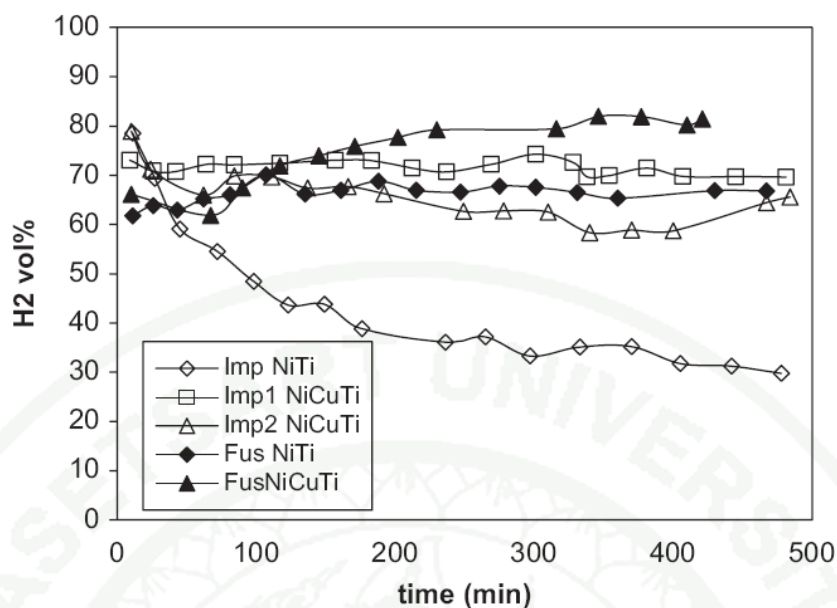


Figure 7 Hydrogen evolution in reactor tests at 700°C with the Ni/TiO₂ and Ni–Cu/TiO₂ catalysts prepared by impregnation and fusion method.

Source: Lázaro *et al.* (2008)

2.2. Nickel-based catalyst for methane cracking reaction

Non-catalytic methane cracking reaction is very slow reaction and required high energy, leading to high operating temperature (1,000°C) as reported in the literature (Ermakova *et al.*, 2000). Therefore, the catalysts were applied in order to reduce the activation energy and fasten the rate of methane cracking reaction.

Many researches were reported that transition metal catalysts such as Ni, Fe, Pd, Co and Mo which able to produce filamentous carbon (Villacampa *et al.*, 2003), carbon nanotubes (CNT) (Niu and Fang, 2007) and carbon nanofibers (CNF) (Ichioka *et al.*, 2007) were appropriate to methane cracking reaction. Among these metal catalysts, nickel was more selected than the other metals due to its low cost and high activity for CNT and hydrogen production (Pompeo *et al.*, 2009). Moreover, the amount of carbon obtained with high-loading metal catalysts decreased in an order of

Ni > Co > Fe. This could be explained that the enthalpy of surface carbide of Ni is 4 KJ/mol, leading to the ease of carbonaceous filament nucleation than those of Co and Fe which has an enthalpy of -50 and -117 KJ/mol, respectively (Avdeeva *et al.*, 2002).

Venugapol *et al.* (2007) studied the effect of nickel content on methane conversion by using 5 – 90 wt.% of nickel loaded on the silica support. They found that the increase of nickel loading had a positive effect on methane conversion and the catalyst stability until the maximum loading of 30 wt.% was reached. The nickel percentage beyond 30 wt.% gave a poorer methane conversion and less catalyst stability, as shown in Figure 8. As a result, the catalyst activity is not a linear function of the nickel amount on the support.

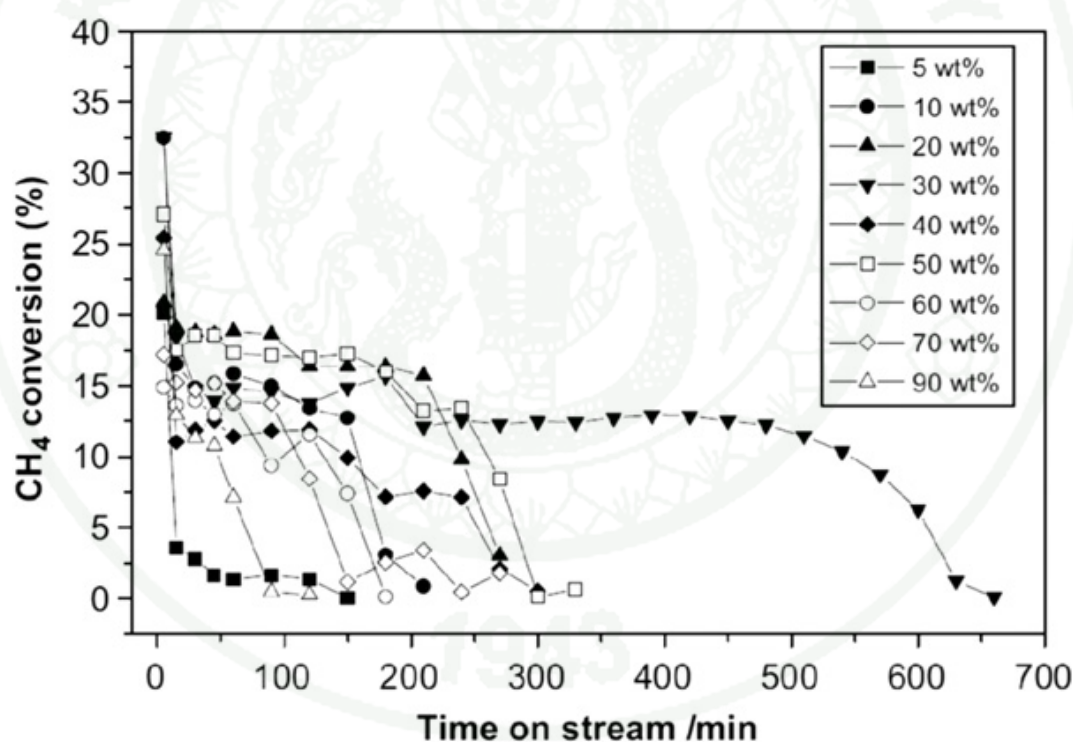


Figure8 Methane conversion over different nickel content supported on SiO₂ catalysts at 600°C.

Source: Venugopal *et al.* (2007)

The catalyst deactivation was the major problem for nickel-based catalysts. The catalyst deactivation could be occurred from several reasons such as poisoning, fouling or coking, sintering and mechanical degradation. However, the main deactivation mechanism during methane catalytic cracking is coking. Coking might affect catalyst activity in several ways as follows (Bartholomew and Robert, 2005):

1. Strongly adsorb on the active phase surrounding and blocking access to the active phase surface
2. Encapsulate the active metal particle
3. Plug the micro and mesopores, denying access to the active phase inside the pores
4. Accumulate as strong carbon filaments, leading to catalyst pellet disintegration
5. In extreme cases, physically block the reactor.

Accordingly, Zhang and Amiridis (1998) concluded that deactivation of nickel-supported catalyst occurred due to the space limitation. As carbonaceous filament began to interfere with each other, the deactivation was occurred.

Many researchers used the mixed metal such as Ni mixed with copper and iron to solve the deactivation problem. Chesnokov and Chikan (2009) developed a 70% Ni - 10% Cu - 10% Fe/Al₂O₃ catalyst for methane cracking reaction. They found that the addition of copper and iron could increase the optimal operating temperature range from 600 to 675°C and from 700 to 750°C for iron and copper, respectively while the stability of catalyst was remained good result. Moreover, Lázaro *et al.* (2008) used copper as a promoter for Ni/TiO₂ catalyst. They found that copper slightly increased catalytic stability compared to those of unpromoted catalyst, as shown in Figure 12.

3. Supported catalysts for methane cracking reaction

Methane conversion was also affected from support catalysts as well as metal catalysts and operating temperatures. This section describes the basic of support preparation, especially sol-gel method, the data of monomodal porous supports for methane cracking reaction and fundamentals of bimodal porous supports.

3.1. Sol-gel method

The sol-gel technique is a popular method to synthesize the porous materials. The sol-gel technique is a transformation of liquid sol (colloid) to a solid gel phase. Moreover, the various porous materials can be synthesized under appropriate drying methods as shown in the Figure 9 (Brinker and Scherer, 1990).

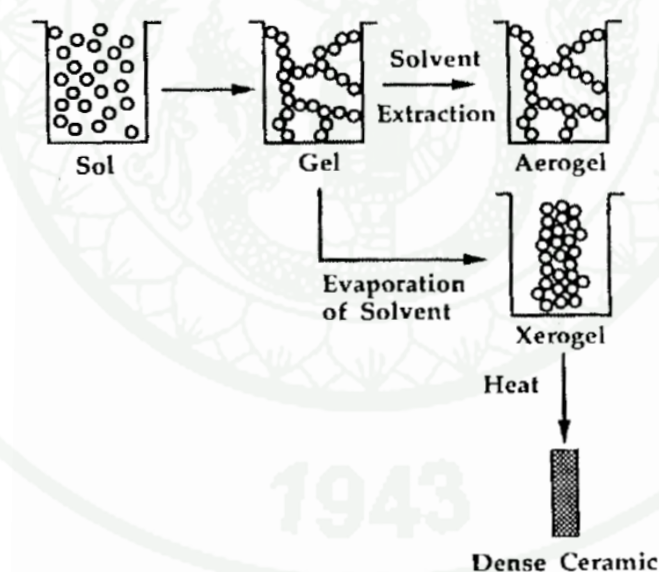
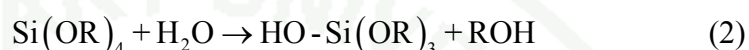


Figure 9 Over view of sol-gel process.

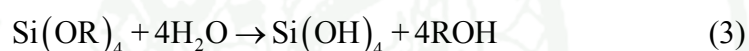
Source: Brinker and Scherer (1990)

The colloid of sol-gel process is prepared by using the precursor, which is metal or metalloid element surround by various ligands (Brinker and Scherer, 1990).

For example, the aluminium sol was normally prepared by using either inorganic salts or organic compounds, which are $\text{Al}(\text{NO}_3)_3$ and $\text{Al}(\text{OC}_4\text{H}_9)_2$, respectively. In the case of inorganic compound, it is widely used as precursor in sol-gel process. Metal alkoxides (inorganic compounds) are the most selected because they react readily with water, which called hydrolysis reaction. The hydrolysis reaction is the reaction that hydroxyl ion attaches to the metal atom, as the reaction shown below:

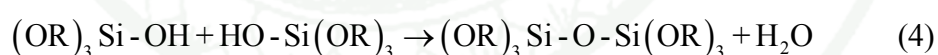


According to the amount of water and catalyst, the hydrolysis reaction will completely react, making all of OR groups are replaced by the hydroxyl group, as the reaction shown below:



Or the hydrolysis may be only partially hydrolyzed, $\text{Si}(\text{OR})_{4-n}(\text{OH})_n$.

Two partially hydrolyzed molecules can link together in a condensation reaction, such as



or



Condensation process can release water or alcohol molecules. This reaction can produce a larger and larger silicon molecules by polymerization process. The polymerization consists of three stages: (1) Polymerization of monomer to form particles, (2) Growth of particles and (3) Linking of particles into chains, then

networks will extend throughout the liquid medium, thickening it to a gel. The condensation diagram is shown in Figure 10 (Brinker and Scherer, 1990).

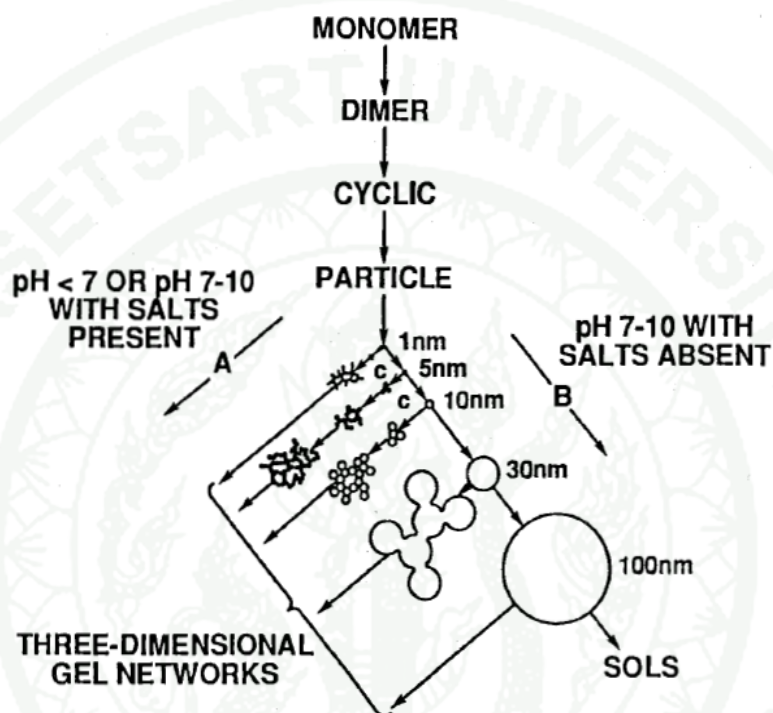


Figure 10 Polymerization behavior of silica: (A) in acid solution or a presence of flocculating salts, particles aggregate into three-dimensional networks and form gels; (B) in basic solution particles in sol grow in size with decrease in numbers.

Source: Brinker and Scherer (1990)

3.2. Silica catalysts for methane cracking reaction

Silica (SiO_2) is widely used as a support for methane cracking reaction due to its low metal-support interaction and large pore (Ermokova *et al.*, 2000). Echegoyen *et al.* (2007) found that minimal interaction between the active metal and

support was important for increasing CH_4 conversion which was in agreement with Takenaka *et al.* (2001).

Ermakova *et al.* (2000) studied the effect of operating temperature to CH_4 conversion over Ni/SiO_2 catalyst, as shown Figure 11. The high catalyst stability was observed with the low operating temperature of 500°C . Moreover, the maximum CH_4 conversion was observed from high temperature (600°C). Furthermore, the moderate temperature (550°C) gave the acceptable CH_4 conversion and stability.

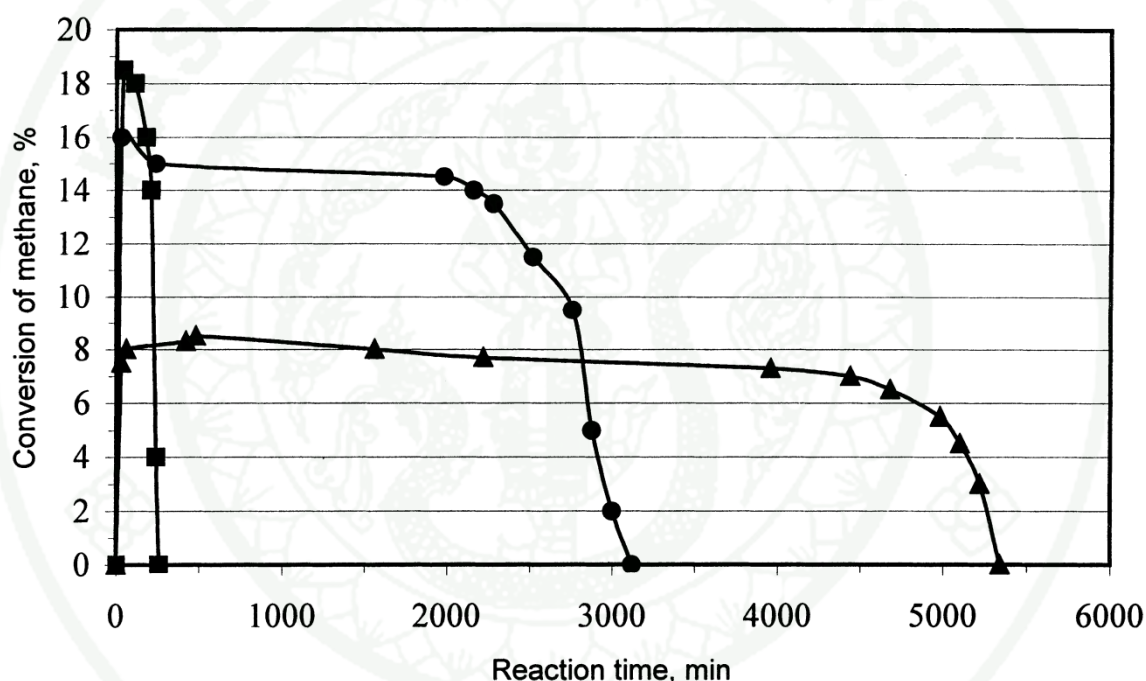
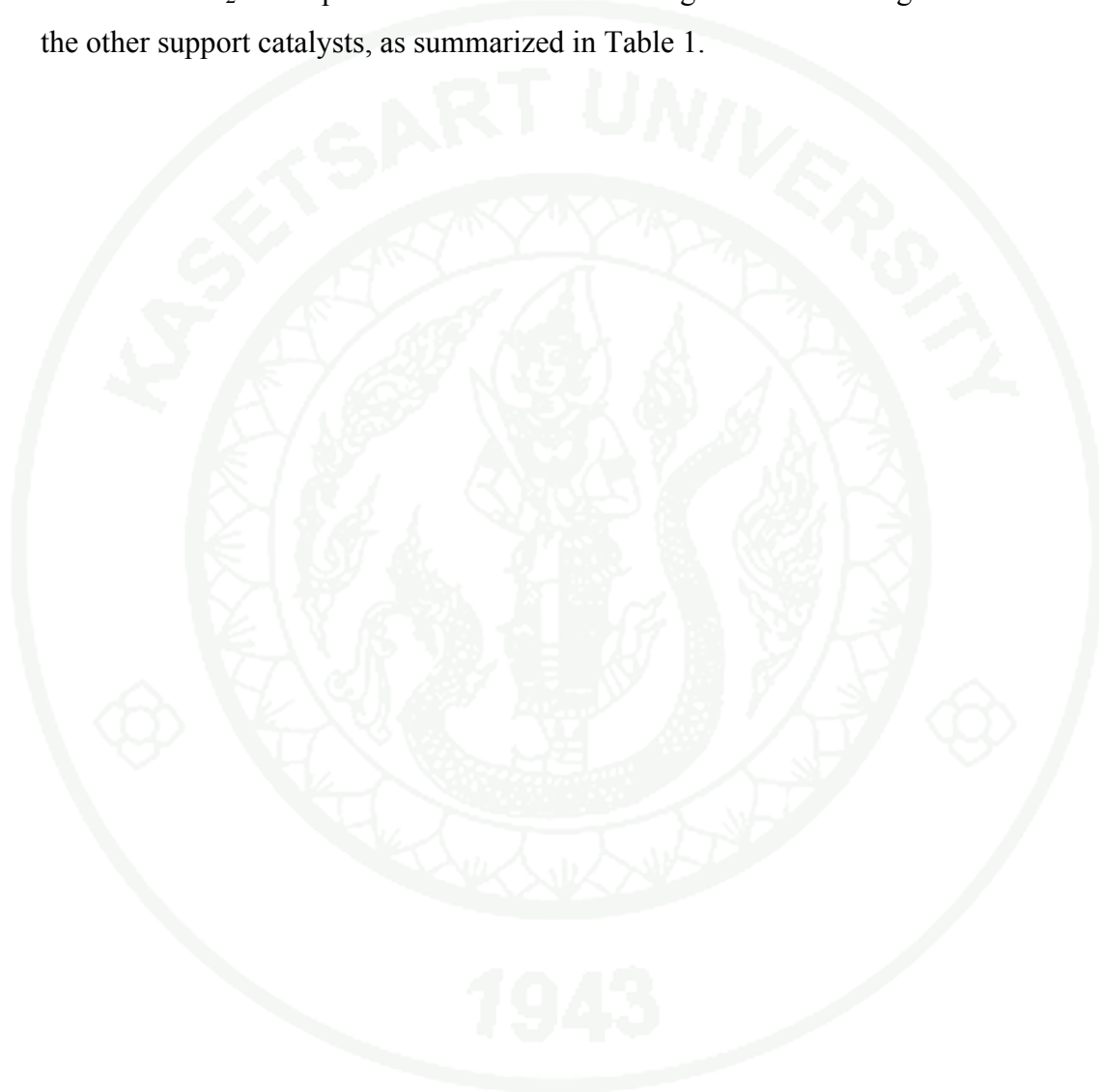


Figure 11 Methane conversion over Ni/SiO_2 at 600°C (■), 550°C (●) and 500°C (▲).

Source: Ermakova *et al.* (2000)

The other types of support catalysts including TiO_2 , Al_2O_3 and MgO had also been reported. Among these supports, TiO_2 was the most active support than the other support catalysts. Lázaro *et al.* (2008) used Ni/TiO_2 and $\text{Ni-Cu}/\text{TiO}_2$ to investigate the effect of calcination temperature over hydrogen production. They

found that the calcination temperature had a slight effect on the hydrogen production of both promoted and unpromoted catalysts as shown in Figure 12. However, at high calcination temperature (800-1,000°C), the strong interaction between nickel and titania was observed, leading to the lower stability. Moreover, Sharif *et al.* (2004) found that TiO₂ could perform the methane cracking reaction for longer life time than the other support catalysts, as summarized in Table 1.



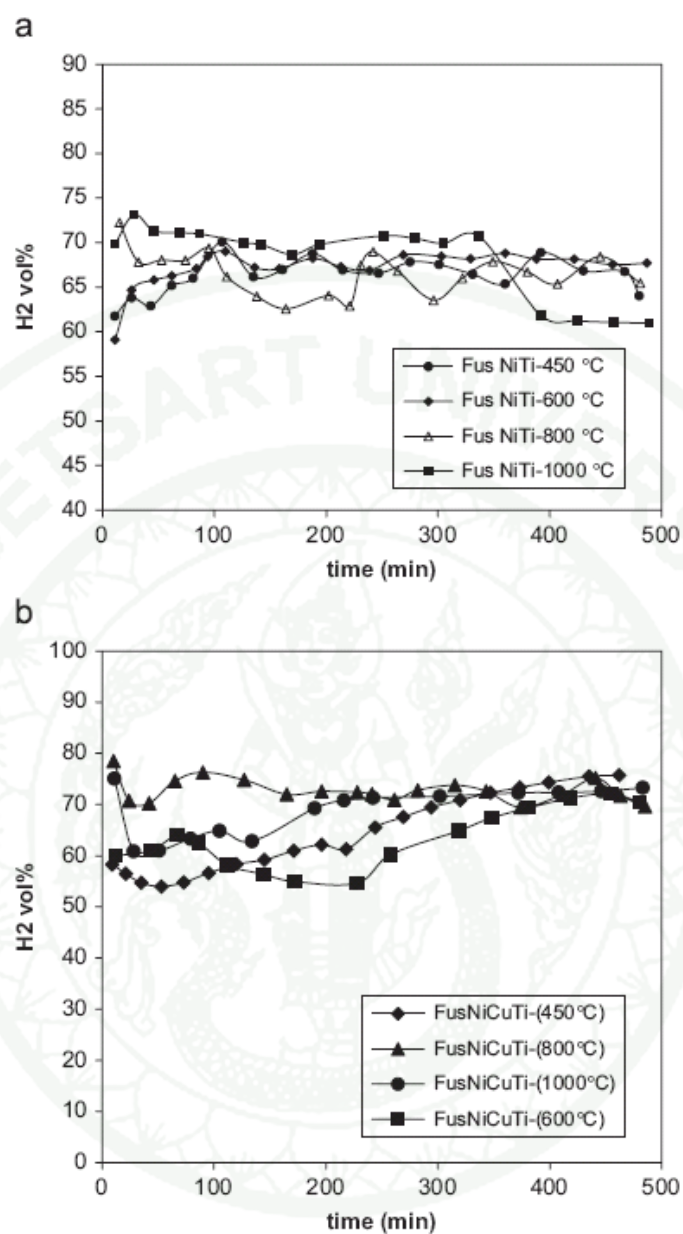


Figure 12 Hydrogen evolution with the fusion catalysts calcined at different temperatures (a) Ni-Ti catalysts and (b) Ni-Cu-Ti catalysts.

Source: Lázaro *et al.* (2008)

Table 1 Details of conversions obtained in the present study with different supports at 998 K and 2700 h⁻¹GHSV

Catalyst	Conversion (%)			
	2 min	5 min	60 min	120 min
13 wt.% Ni/SiO ₂	97.41	74.12	48.67	PB ^a
13 wt.% Ni/Al ₂ O ₃	99.54	72.98	PB ^a	PB ^a
13 wt.% Ni/TiO ₂	99.18	64.57	61.34	62.44
13 wt.% Ni/MgO	99.23	52.23	15.84	8.05

^apressure buildup

Source: Sharif *et al.* (2004)

Takenaka *et al.* (2001) also studied the effect of support including SiO₂, TiO₂, graphite, MgO, Al₂O₃ and SiO₂.MgO on the performance of methane cracking reaction. They found that SiO₂, TiO₂ and graphite exhibited a longer lifetime and higher catalytic activities than those of MgO, Al₂O₃ and SiO₂.MgO supports. However, SiO₂ showed the better conversion than those of TiO₂, as shown in Figure 13. This result was not agreement with the results of Lázaro *et al.* (2008) and Sharif *et al.* (2004).

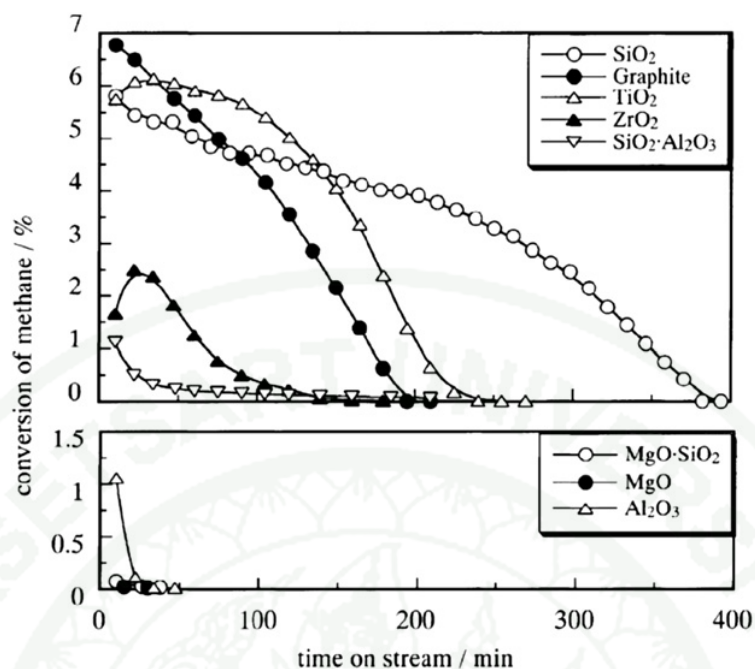


Figure 13 Methane conversion over Ni catalysts supported on different supports at 500°C.

Source: Takenaka *et al.* (2001)

Moreover, Takenaka and his co-workers (2001) also studied the electronic state of nickel particle supported on active supports including SiO₂, TiO₂ and graphite and inactive supports consisting of MgO, Al₂O₃ and SiO₂.MgO by using X-ray diffraction (XRD) technique as shown in Figure 14. The results showed that nickel species loaded on active supports were crystallite nickel particles. On the other hand, nickel on inactive supports was amorphous nickel. Therefore, the latter group of supports could not catalyze the methane cracking reaction.

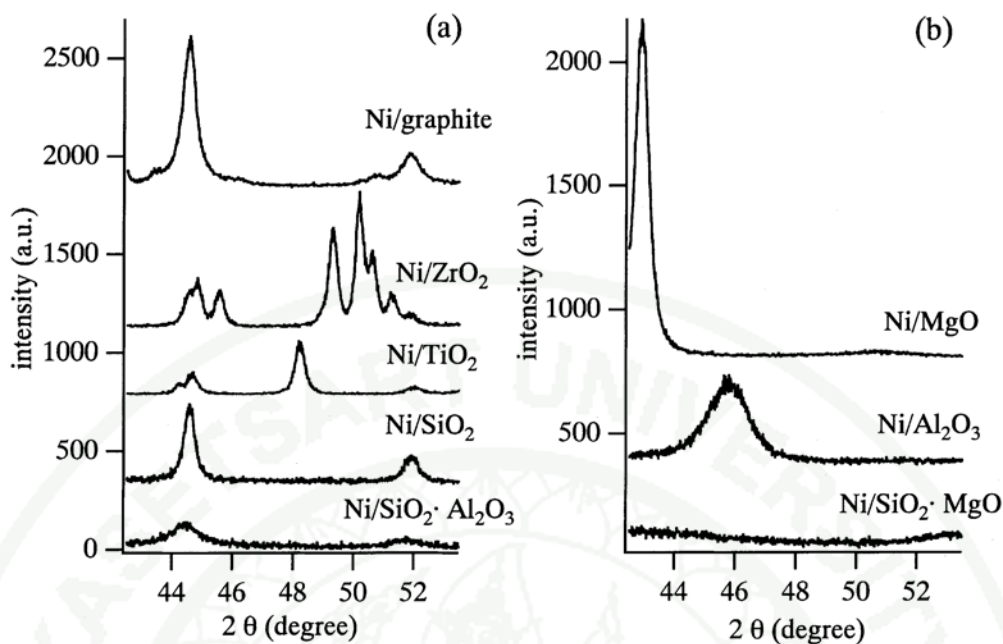


Figure 14 XRD patterns of supported-Ni catalysts.

Source: Takenaka *et al.* (2001)

3.2 Bimodal support for Fischer-Tropsch synthesis (FTS)

There are various ways to synthesize the bimodal porous materials such as incipient-wetness impregnation (Shinoda *et al.*, 2004), two templates technique (Jullaphan *et al.*, 2009) and one template technique via sol-gel method (Witoon *et al.*, 2008). A simple preparation method of bimodal pore supports of a commercially available silica gel (Q-50) synthesized by incipient-wetness impregnation with metal oxide sol is schematically shown in Figure 15. The pore size distributions of catalysts obtained from N₂-physisorption, exhibit two narrow pores, which clearly confirmed the pore structure of bimodal porous materials (Shinoda *et al.*, 2004), as shown in Figure 16.

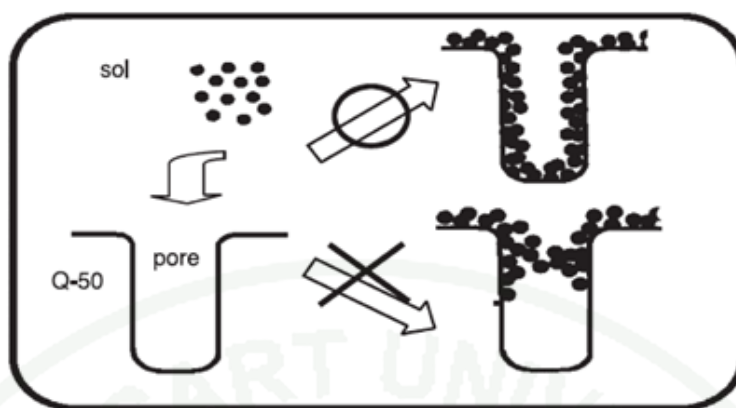


Figure 15 Formation scheme of the bimodal pore support.

Source: Shinoda *et al.* (2004)

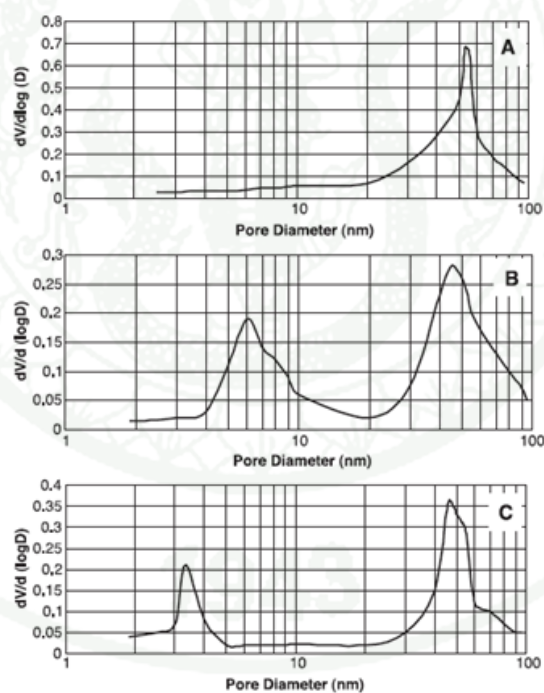


Figure 16 Pore size distribution of Q-50 and the bimodal porous supports: (A) silicaQ-50 (B) bimodal porous silica support (C) Zr/bimodal porous support.

Source: Shinoda *et al.* (2004)

The bimodal porous materials also can be synthesized by sol-gel method using specific templates which various structures and combinations such as the combination of micropore (<2 nm) and mesopore (2-50 nm), the small-mesopore and large-mesopore, and mesopore and macropore (>50 nm). The bimodal porous material containing micropore and mesopore structures was successfully synthesized by Witoon *et al.* (2008). They used chitosan as template and then adjusted the pH of mixture to 2. At this pH value, chitosan template would dissolve to small molecules. Therefore, the small interparticle channels between nonporous silica particles would be obtained after chitosan template was removed by calcination process.

The other combinations between mesoporous and mesoporous structures of different sizes were also synthesized. Jullaphan *et al.* (2009) successfully synthesized bimodal small-mesopore and large-mesopore by the mixed-templating technique. Pluronic P123 (P123: PEO₂₀PPO₇₀PEO₂₀) and CTAB (C₁₆H₃₃N(CH₃)₃Br) were used as the dual pore structure-directing agents for bimodal mesoporous silica synthesis, respectively. The mixture of CTAB was added to SBA-15 gel solution synthesized using Pluronic P123 as the primary template and reacted with free sodium silicate. The as-synthesized bimodal porous silica revealed the mixed-phase uniformly infiltrated SBA-3-like in SBA-15 bimodal mesoporous silica as shown in Figure 17 (Jullaphan *et al.*, 2009).

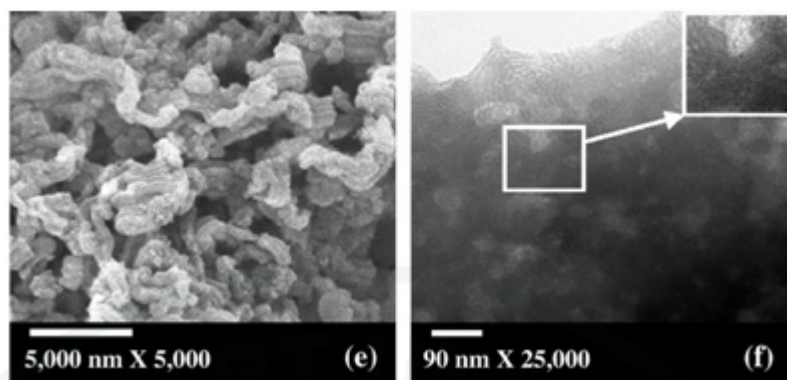


Figure 17 SEM images (a) and TEM images (b) of mixed-phase bimodal mesoporous silicas.

Source: Jullphan *et al.* (2009)

Furthermore, the meso-macroporous silica could also be synthesized by sol-gel technique with the addition of template to create the phase separation in the gel product. Takahashi *et al.* (2007) used poly(ethylene oxide) or PEO as a template. The size of macropore was controlled by adjusting the pH of mixture. The other template possibly used for bimodal porous silica synthesis is chitosan. Witoon *et al.* (2008) added chitosan into sodium silicate solution and the pH of mixture was adjusted to increase the size of macropore. The TEM images of bimodal meso-macroporous silica with adjusting pH are shown in Figure 18.

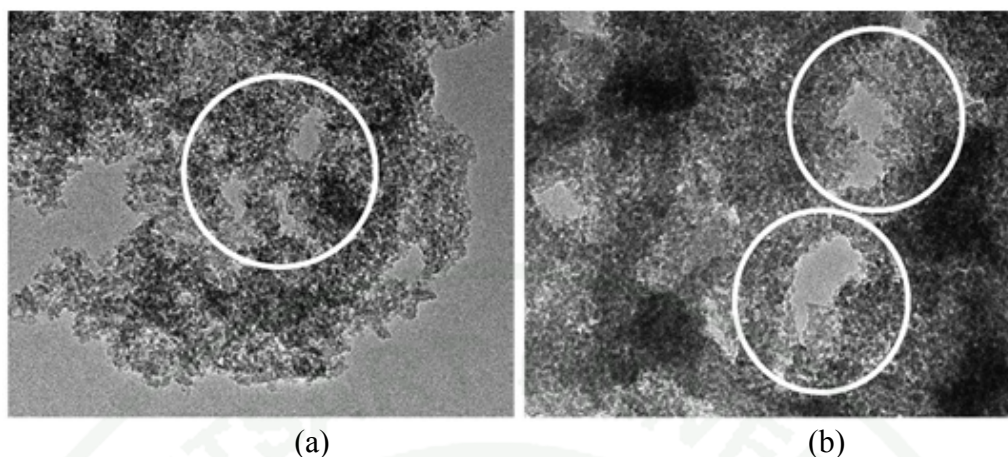


Figure 18 TEM image of meso-macroporous silica with adjusting pH (a) pH = 3 and (b) pH = 5.

Source: Witoon *et al.* (2008)

As mentioned above, the deactivation of nickel supported catalysts was the space limitation or known as pore blockage by carbon nanotubes produced from methane cracking reaction. Therefore, bimodal structures containing mesopore and macropore structures could possibly solve the pore blockage problem. In this research, bimodal porous silica supports including mesopore and macropore structures was synthesized following Witoon *et al.* (2008) and used as nickel supported catalysts. The monomodal porous silica supports were also synthesized to compare the effect of bimodal mesoporous silica. The physical and chemical properties of nickel supported catalysts and their catalytic performances were also investigated.

MATERIAL AND METHOD

The effect of bimodal porous silica to the carbonaceous filament synthesis was investigated through methane cracking reaction. The bimodal porous silica (BS) and monomodal porous silica (MS) supports were synthesized. The details of equipments and support syntheses were shown as follows:

Synthesis of nickel supported porous silica

1. Equipments of Monomodal and Bimodal Porous Silica Synthesis

- 1.1. Digital hot plate and stirrer (Schott, SLR)
- 1.2. Magnetic hot plate and stirrer (Schott, SLR)
- 1.3. Furnace (Carbolite, ELF10/6)
- 1.4. Digital balance (Metler Toledo, AT 400)
- 1.5. Hot air oven (Binder, ED53)
- 1.6. Autoclave (made by order)

2. Materials of Monomodal and Bimodal Porous Silica Synthesis

- 2.1 Rice husk ash
- 2.2 Chitosan (Eland Corporation, 90.0 % deacetylation)
- 2.3 Pluronic P123(PEO₂₀PPO₇₀PEO₂₀: Aldrich; Product code No. 435-465)
- 2.4 Cetyltrimethyl ammonium bromide (C₁₆H₃₃N (CH₃)₃-Br, CTAB: AJAX, No. A147)
- 2.5 Sodium hydroxide (NaOH: Merck; Purity, 99.0 %)
- 2.6 Hydrochloric acid (HCl: J.T. Baker; Purity, 36.5 -38.0 wt. %)
- 2.7 Acetic acid, CH₃COOH (CH₃COOH: BDH; Purity, 100%)
- 2.8 Cobalt nitrate (Co(NO₃)₂·6H₂O, 99.0% purity, UNIVAR)
- 2.9 Distilled water

3. Monomodal and Bimodal Porous Silica Synthesis

In order to synthesize bimodal and monomodal porous silica, rice husk ash-derived sodium silicate was firstly prepared according to Chareonpanich *et al.* (2004) and used as the silica source for bimodal and monomodal porous silica synthesis. The monomodal porous silica supports were synthesized via sol-gel method. After that, the bimodal porous silica products were then synthesized by using sol-gel method and macropores structure was created by chitosan template. The preparation of sodium silicate from rice husk ash, monomodal and bimodal porous silica products were shown as follows:

3.1 Preparation of sodium silicate from rice husk ash

Sodium silicate solution ($\text{Na}_2\text{Si}_3\text{O}_7$: 4 wt.% NaOH; 27 wt.% SiO_2) was prepared from rice husk ash (based on 99.7 wt.% silica). In this stage, 1 g of rice husk ash was dissolved in 7.40 mL of 1 M NaOH solution. The obtained mixture was stirred at approximately 80°C until rice husk ash was completely dissolved and the clear solution of sodium silicate was obtained. The volume of mixture was one half reduced in order to obtain the desired composition of sodium silicate solution by simple evaporation (Chareonpanich *et al.*, 2004). Sodium silicate synthesis scheme is summarized as shown in Figure 19.

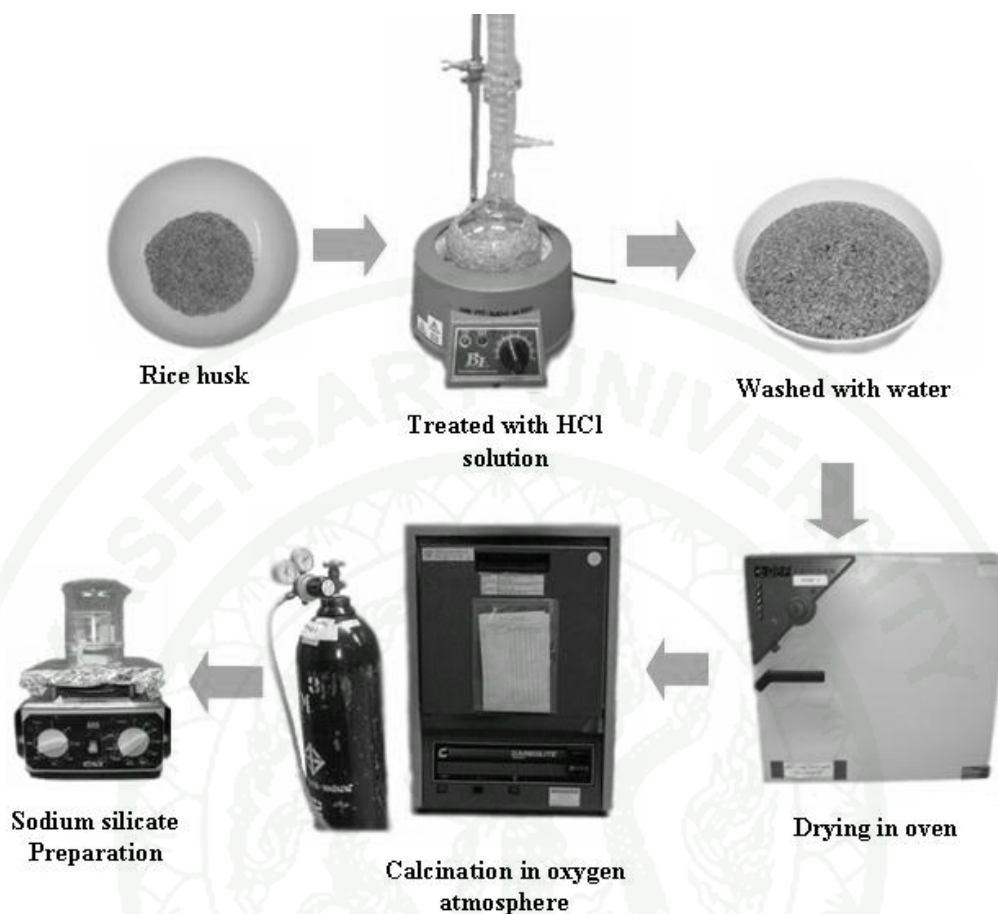


Figure 19 Schematic diagram of sodium silicate synthesis process.

3.2 Monomodal porous silica syntheses

The monomodal porous silica products, xerogel with pH of solution at 3 and 5, were synthesized in order to compare the results with those of the bimodal porous silica products.

Sodium silicate solution (based on 1 g of silica) was primarily diluted with 10 ml of deionized water. The pH values of solution were adjusted to 3 and 5. After that, the hydrolysis-condensation reaction was carried out at 40°C for 24 h, and then the resultant solution was aged in the Teflon-lined autoclave at 100°C for 24 h. The solid products were filtrated, washed several times with distilled water, dried at

120°C for 24 h and calcined in air at 550°C for 5 h at the heating rate of 5°C/min. The nomenclatures were listed in Table 2.

3.3 Bimodal porous silica syntheses

The porous structures of bimodal porous silica were the combination of mesopore and macropore structures, which has the pore diameter below 5 nm and beyond 50 nm, respectively. In this research, methane cracking reaction was performed over the bimodal porous silica supports to study the effect of pore size on carbonaceous filament formation.

A chitosan solution can be prepared by dissolved 1 g of chitosan in 60 ml of 2% v/v acetic acid in deionized water at room temperature. Then, sodium silicate solution (based on the 1 g of silica) was primarily diluted with 10 ml of deionized water and slowly added to the chitosan solution with vigorous stirring. The pH values of solution were adjusted to 3 and 5 with 1 M HCl and 1 M NaOH. After that, the hydrolysis-condensation reaction was carried out at 40°C for 24 h, and then the resultant solution was aged in the Teflon-lined autoclave at 100°C for 24 h. The solid products were filtrated, washed several times with distilled water, dried at 120°C for 24 h and calcined at 550°C for 5 h with the heating rate of 5°C/min. The nomenclatures and synthesis details were listed in Table 2 and the schematic detail of this series of experiment is shown in Figure 20.

1943

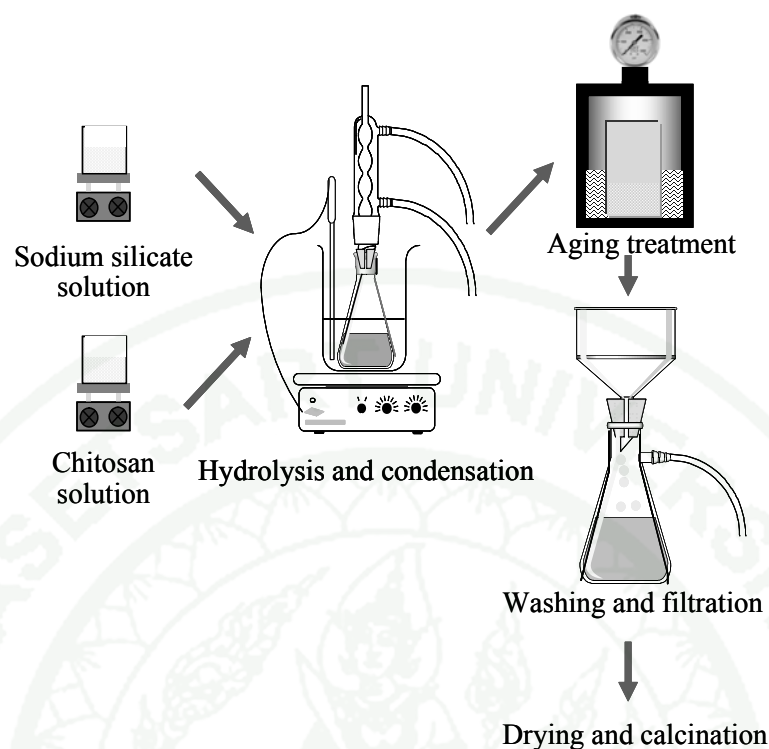


Figure 20 Schematic diagram of bimodal porous silica synthesis.

Table 2 Synthesis conditions for monomodal porous silica supports and bimodal meso-macroporous silica supports.

Sample ID ^a	Synthesis conditions ^b	
	pH of mixture	Chitosan/silica (g/g)
MS-1	3	0
MS-2	5	0
BS-1	3	1
BS-2	5	1

^a Porous silica products were prepared without (MS-X) and with (BS-X) chitosan template, where X is the pH of mixture.

^b The aging temperature and calcined temperature were fixed at 100°C and 550°C, respectively throughout this series of experiment.

4. Loading of Nickel Metal onto Monomodal and Bimodal Porous Silica Supports

Nickel metal of 5 wt.% was loaded onto 0.5 g of monomodal and bimodal porous silica supports via incipient wetness impregnation method. The solution of metal precursor was prepared by dissolving certain amount of nickel nitrate ($\text{Ni}(\text{NO}_3)_2 \cdot 6\text{H}_2\text{O}$) in a required amount of distilled water under stirring. The obtained products were dried at 120°C for 24 h and calcined in air at 550°C for 5 h. The nickel loaded on monomodal and bimodal porous silica catalysts were obtained and denoted as Ni/MS-1, Ni/MS-2, Ni/BS-1 and Ni/BS-2.

5. Characterization of Monomodal and Bimodal Porous Silica

5.1 N_2 -sorption measurement

BET surface area, sorption isotherms, pore size distribution, and pore volume of monomodal and bimodal porous silica products were analyzed by using N_2 -sorption equipment of Quantachrome Corporation (Model: Autosorb1). Prior to each measurement, samples were degassed at 200°C under vacuum and followed by flowing helium gas to remove adsorbed water and other volatile matters from the surface of solid samples. The measurement was done at high vacuum level (10^{-4}Torr) at the temperature of liquid N_2 (-196°C) using the total N_2 adsorption/desorption points of 55 points.

5.2 Scanning electron microscopy (SEM)

Surface morphology and silica cluster size of porous silica products were examined by using JEOL JSM6301-F. The powder sample was attached on a carbon tape over alumina specimen mount, and coated with gold (Au) using a sputtering technique.

5.3 X-ray powder diffraction (XRD)

X-ray powder diffraction measurement was performed at room temperature using a Phillips powder diffractometer with monochromatized Cu-K α radiation. Cobalt phases were detected by comparing the diffraction patterns with those of the standard powder XRD file compiled by the joint committee on powder diffraction standards (JCPDS) published by the International Center for Diffraction Data. The NiO crystallite diameters were calculated by using Scherrer equation (as shown below) from the most intense NiO peak at 2θ of 43.2.

$$d = \frac{0.89\lambda}{B \cos \theta} \times \frac{180^\circ}{\pi} \quad (6)$$

where

d is the mean crystallite diameter

λ is the X-ray wave length (1.54 Å)

B is the full width half maximum (FWHM) of the NiO diffraction peak.

Performance Test for Methane Cracking Reaction

1. Equipments of Methane Cracking Reaction

1.1. Pressure regulator

1.2. Mass flow controller (8300 Series, KOFLOC)

1.3. Thermocouple (K-type)

1.4. Tube furnace (CFW 1300, Carbolite)

1.5. Bubble flow meter

1.6. Gas chromatograph equipped with thermal conductivity detector (TCD)

and chromatopac data processor (GC-2014, Shimadzu)

2. The Methane Cracking Reaction

The catalytic performance unit for the methane cracking reaction is shown in Figure 21. This experimental unit consists of a feed flow measuring and controlling system, a furnace equipped with inconel tube reactor and a sampling system. The catalytic reaction testing unit was designed to operate under high temperature and atmospheric pressure conditions. The details of particular system are explained below.

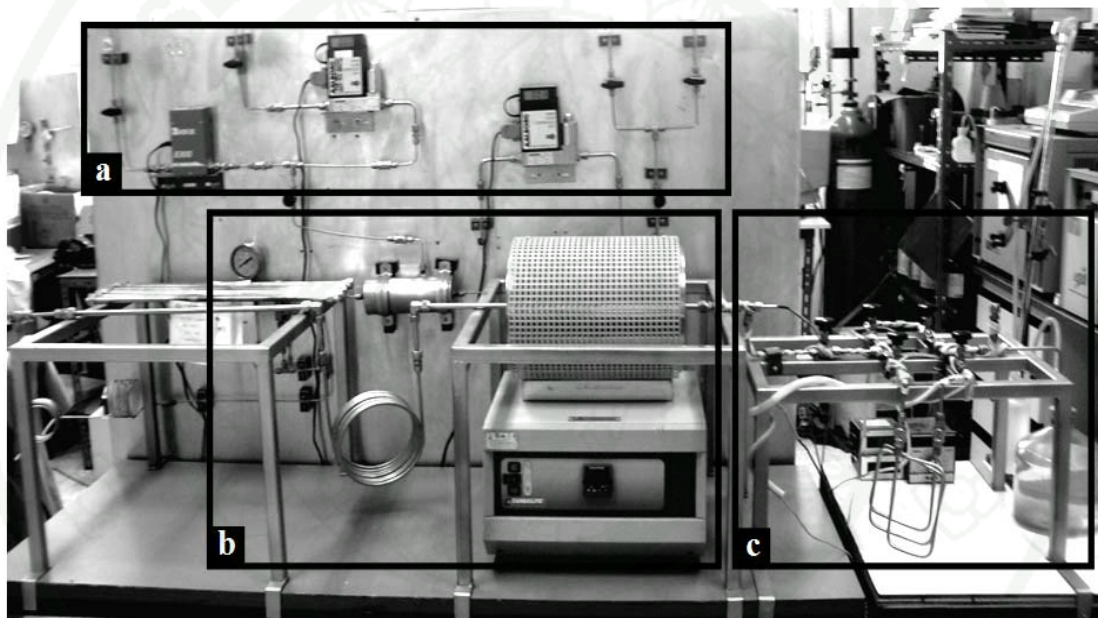


Figure 21 Catalytic reaction testing unit: (a) a feed flow measuring and controlling system, (b) a furnace-equipped stainless steel tube reactor and (c) a sampling system.

2.1 The feed flow measuring and controlling system

In this system, mass flow controllers were used to finely control and indicate the flow rate of feed gases including methane, nitrogen, hydrogen and oxygen. Methane was used as a reactant gas while nitrogen was used to dilute methane gas, hydrogen was used for the catalyst reduction, and oxygen was used for

calcination process. In order to monitor the system leakage, nitrogen gas was also applied. Flow rates of hydrogen, oxygen and nitrogen were measured and controlled by Aalborg mass flow controller (Figure 22).



Figure 22 Mass flow controller(Aalborg GFC thermal mass flow controller)

2.2 The packed bed reactor

The inconel tube of 3/8" I.D. and 45 cm length was used as the packed-bed reactor. At the stage of reaction, the inconel tube was heated with an electric furnace (Figure 23) controlled by the temperature controller. A K-type thermocouple connected to a temperature controller unit was inserted inside the inconel tube in order to measure and control the temperature of the catalyst bed. Catalyst powder was packed in the isothermal zone of tube reactors between quartz wool layers as the scheme shown in Figure 24.



Figure 23 The reactor of methane cracking reaction equipped with the electric heater (Carbolite tube furnace).

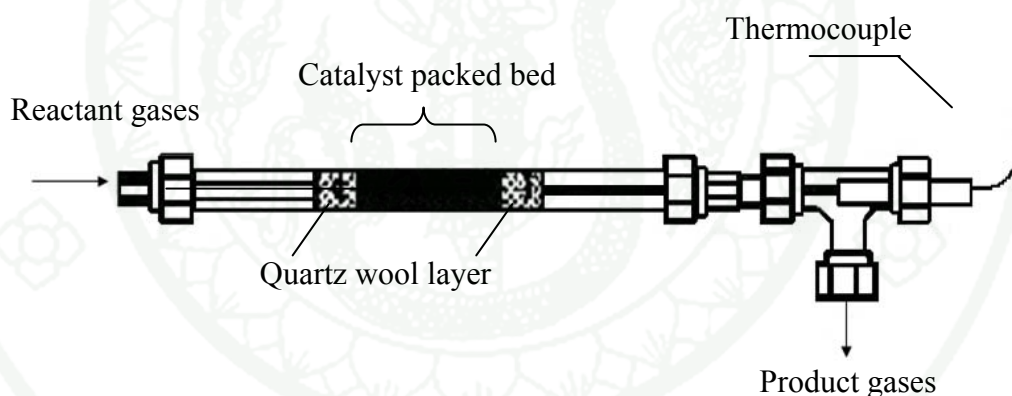


Figure 24 Schematic setup of the stage of methane cracking reaction reactor.

2.3 Gas analysis unit

The gas chromatograph was applied to analyze the inlet and outlet gases. Gas analysis unit (Figure 25) consists of Shimadzu gas chromatograph and chromatopac data processor (GC-2014) equipped with thermal conductivity detector (TCD) was used to quantitatively analyzed amounts of CO and CO₂ (Unibead-C packed column was applied).



Figure 25 Shimadzu gas chromatograph (GC-2014) equipped with thermalconductivity detector (TCD) and chromatopac data processor.

The conditions for CH₄ and H₂ analysis were:

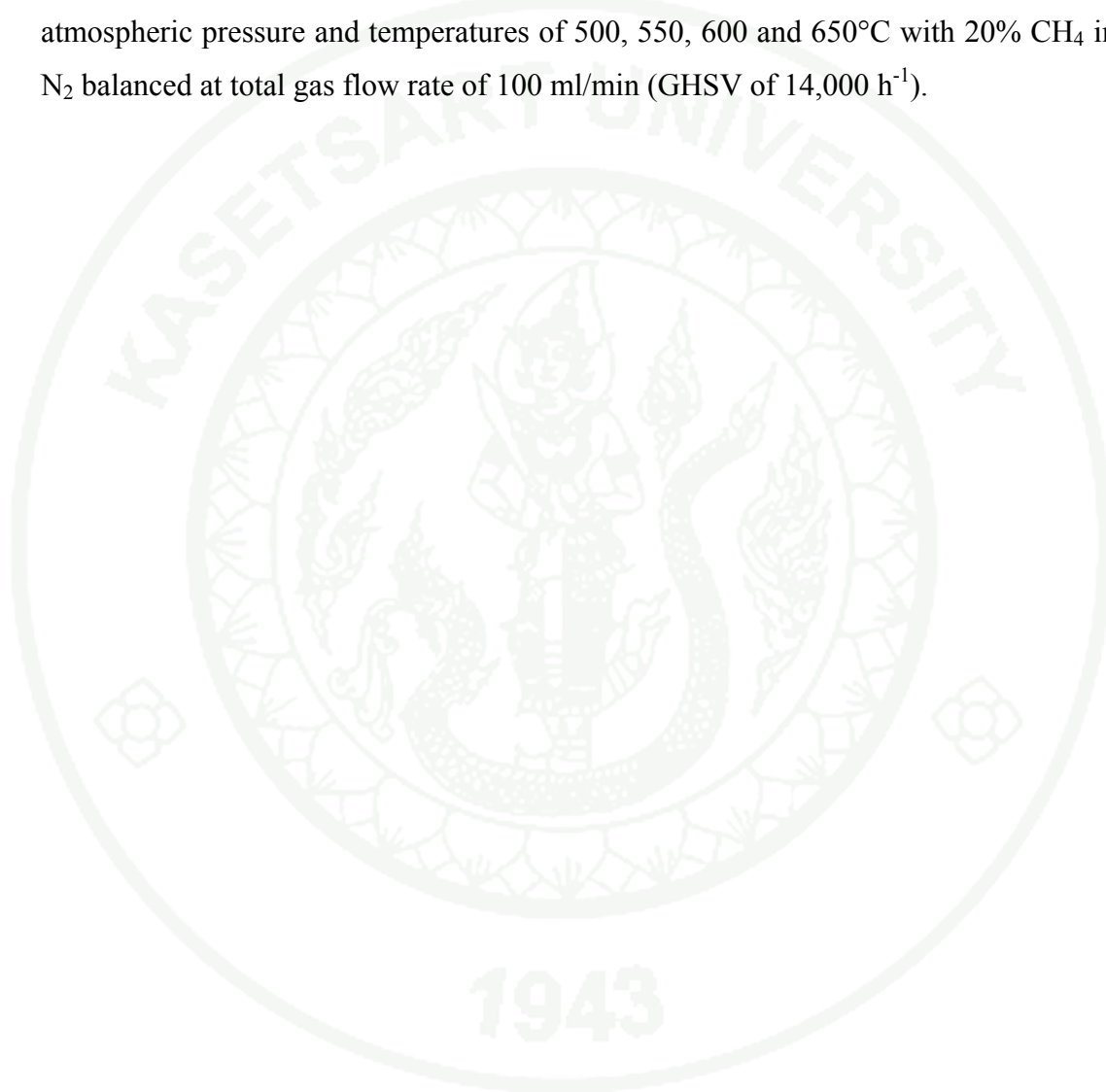
- Initial carrier gas (Ar) flow rate	25	ml/min
- Final carrier gas (Ar) flow rate	25	ml/min
- Injector temperature	150	°C
- Initial column temperature	150	°C
- Final column temperature	150	°C
- Detector temperature (Pre)	150	°C
- Detector temperature	150	°C
- Current	60	mA

2.4 Test for methane cracking reaction

Before testing the catalyst performance, 0.5 g of nickel supported catalyst was thoroughly mixed with 2 g of sand, in order to avoid the effect of poor heat transfer during catalyst testing experiment. The catalyst with sand was packed in inconel tube reactor. To obtain an active form of catalyst (nickel metal), the catalyst was reduced by using H₂ at atmospheric pressure and temperature of 700 °C for 4 h with the flow rate of 60 ml/min (NTP) and then flushed and cooled down with

nitrogen gas. After pretreatment procedure, the catalyst was ready for the catalytic performance test.

During the reaction, CH_4 was decomposed to hydrogen and carbonaceous filaments over nickel-containing monomodal and bimodal catalysts at atmospheric pressure and temperatures of 500, 550, 600 and 650°C with 20% CH_4 in N_2 balanced at total gas flow rate of 100 ml/min (GHSV of 14,000 h^{-1}).



RESULTS AND DISCUSSION

In this present research, monomodal and bimodal porous silica supports of various pore sizes and pore structures were used as nickel metal supports in order to investigate the effect of pore characteristics and operating temperatures on the performance of methane cracking reaction. The catalysts were prepared by using incipient wetness impregnation methods base on 5 wt.% nickel loading. The performances of the obtained catalysts were examined on methane cracking reaction under the conditions of atmospheric pressure, operating temperatures of 500, 550, 600 and 650°C and total flow rate of 100 ml/min with 20% CH₄ mixed with 80% N₂.

The experimental results and discussion were reported as characteristics of nickel supported on monomodal and bimodal porous silica catalysts denoted as Ni/MS-1, Ni/MS-2, Ni/BS-1 and Ni/BS-2 and their catalytic performances on methane cracking reaction, respectively. The physical and chemical properties of catalysts were examined by using N₂-sorption and X-ray diffraction (XRD). Then, the effects of pore structures and operating temperatures on the performances of methane cracking reaction were observed.

1. Physical and Chemical Properties of Catalysts

In this part, the physical and chemical properties including sorption isotherms, pore size distribution, BET surface area, total pore volume, mean pore diameter, surface morphology and aggregates of silica nanoparticles of Ni/MS-1, Ni/MS-2, Ni/BS-1 and Ni/BS-2 were discussed.

N₂-sorption technique was used to investigate the physical properties of monomodal porous silica supports, as shown in Figures 26(a) and (b). In the case of monomodal porous silica supports (Figure 26(a)), type II isotherms indicating the existence of monomodal macroporous structure were observed. Moreover, it found that the capillary condensation steps shifted to higher relative pressures when

increasing pH values due to the increasing in the mean pore size of monomodal porous silica supports.

Composite isotherms between types II and IV were observed in bimodal porous silica supports as shown in Figure 26(b), indicating that bimodal porous silica supports consisted of mesoporous and macroporous structures. Moreover, the capillary condensation steps also shifted to the higher relative pressure as well as monomodal porous silica supports. Therefore, high pH values could increase the relative pressure due to the information of the larger mean pore diameter of bimodal porous silica supports.

Moreover, the physical properties of nickel supported on monomodal and bimodal porous silica supports were also characterized by using N₂-sorption technique, as shown in Figures 26(c) and (d). As a result, the adsorption isotherms of nickel supported on monomodal and bimodal porous silica supports exhibited the same trends as unloaded porous silica supports. However, the volumes of gas adsorbed were decreased when compared to those of unloaded porous silica supports because the pores of porous silica supports were blocked by nickel particles in some extent.

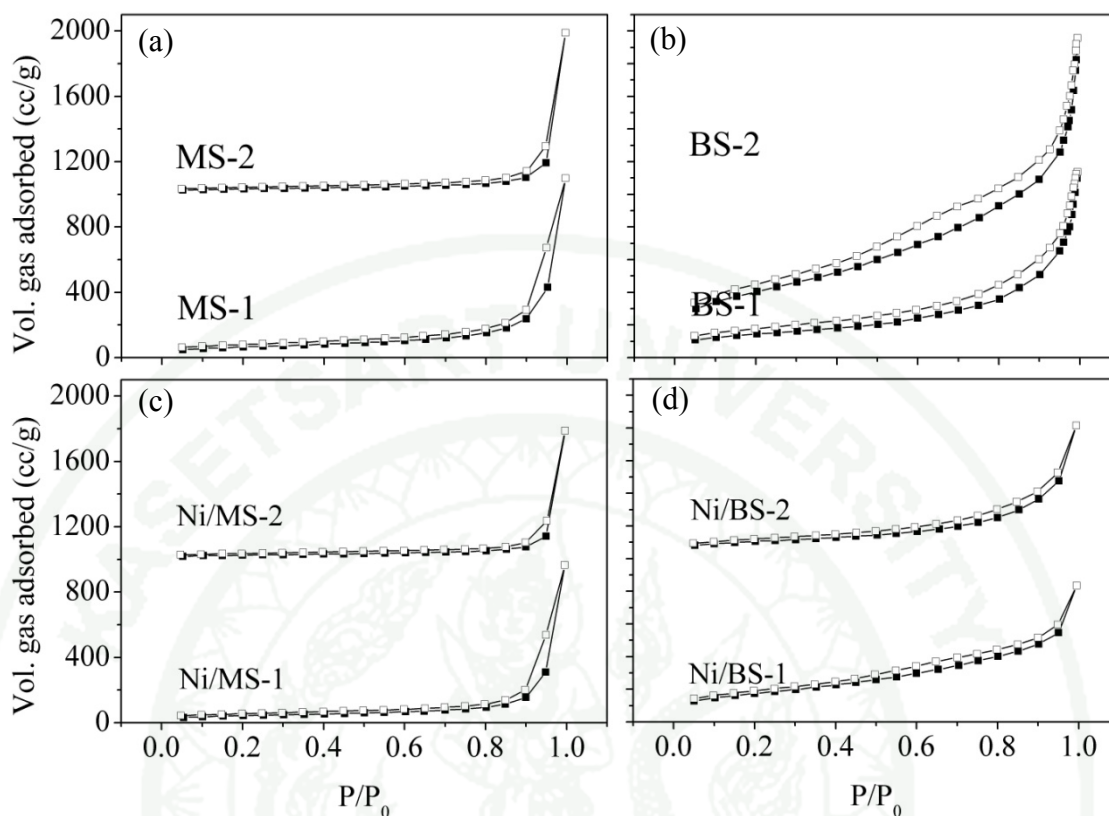


Figure 26 Isotherm of porous silica supports including (a) monomodal and (b) bimodal porous silica supports and nickel supported on porous silica supports including (c) monomodal and (d) bimodal porous silica supports.

As shown in Figures 27(a) and (b), the porous silica supports without chitosan template exhibited a single peak, indicating the existence of monomodal porous silica supports with the mean pore diameter of 29.54 and 54.91 nm for MS-1 and MS-2 respectively, as shown in Table 3. Moreover, the porous silica supports with chitosan template showed two main peaks at 3-5 nm and 40-60 nm, as can be seen in Figures 27(c) and (d). BS-1 and BS-2 supports were bimodal porous silica supports. Furthermore, pore size distributions of nickel supported on monomodal and bimodal porous silica supports are shown in Figure 28. The similar results as unloaded catalysts were observed.

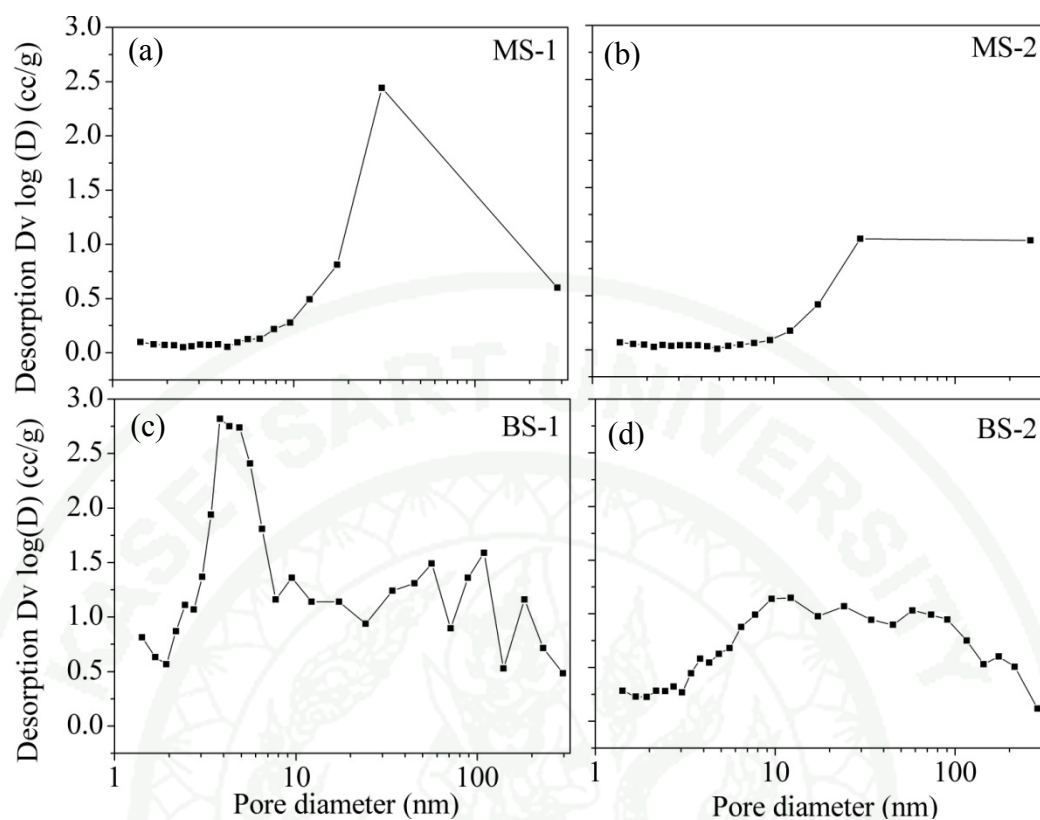


Figure 27 Pore size distributions of (a) MS-1, (b) MS-2, (c) BS-1 and (d) BS-2.

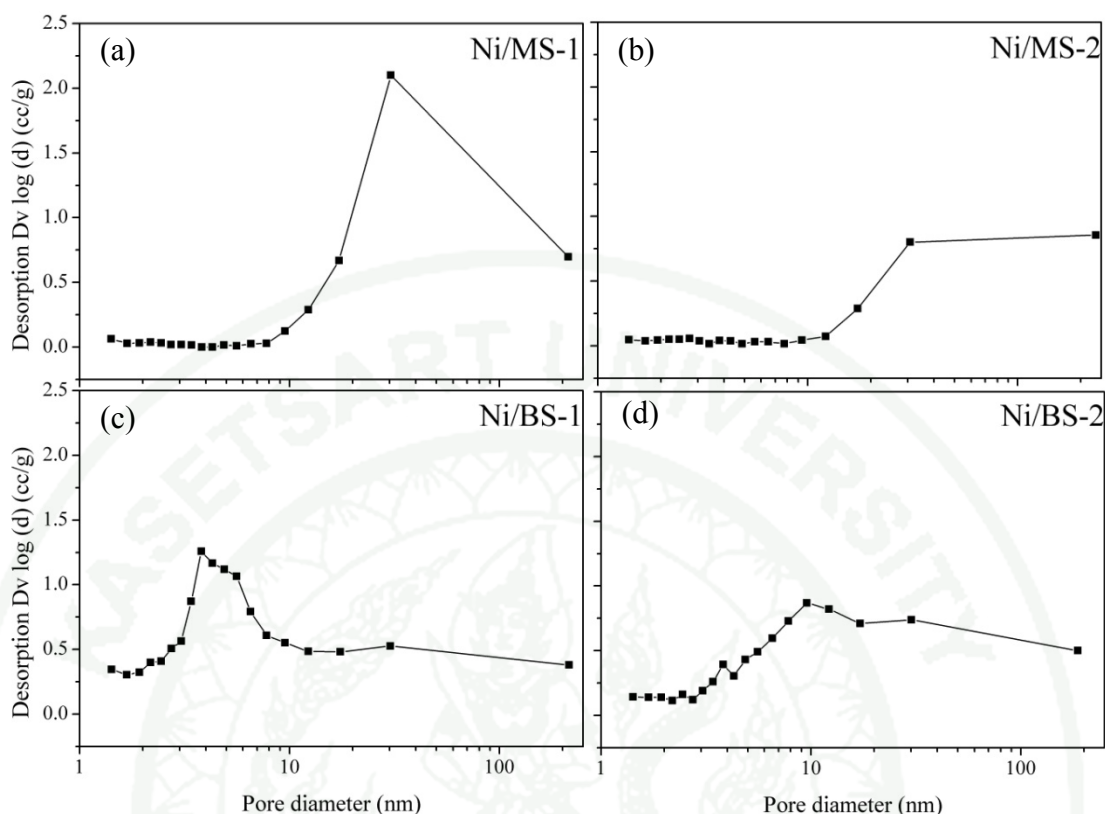


Figure 28 Pore size distributions of (a) Ni/MS-1, (b) Ni/MS-2, (c) Ni/BS-1 and (d) Ni/BS-2 catalysts.

The BET surface area, BJH pore diameter and total pore volume of the porous silica products synthesized without and with chitosan template of different pH values are shown in Table 3. In the case of monomodal porous silica supports, MS-2 showed the lower BET surface area but higher total pore volume and average pore diameter when compared to those of MS-1 because at high pH value, silanol groups (Si-OH) of SiO₂ repelled with each other, leading to the large total pore volume and average pore diameter. For bimodal porous silica supports, the similar trends of the results were obtained. However, BET surface area of bimodal porous silica supports were higher than that of the monomodal porous silica supports because mesopore of bimodal porous silica supports could enhance the BET surface area and reduced the total pore volume and average pore diameter. After nickel loading, the BET surface area, BJH pore diameter and total pore volume of nickel supported on monomodal and bimodal

porous silica showed the similar trends of results as the unloaded porous silica supports but the lower values were obtained. It could be explained that nickel particles could partially block the pores of porous silica supports, leading to the decrease of BET surface area, BJH pore diameter and total pore volume. When considered Ni/MS-1 catalyst, total pore volume was slightly lower than that of MS-1 even though nickel was loaded on MS-1 support. It should be explained that nickel particles were agglomerated with each other and created another pore on MS-1 support, leading to the slightly decrease of total pore volume and increase of average pore diameter of Ni/MS-1 when compared to that of MS-1 support.

Table 3 Physical properties of loaded and unloaded monomodal porous silica supports

Samples	BET (m ² /g)	Total pore volume (cc/g)	Average pore Diameter (nm)	NiO Crystallite Diameter (nm)
Unloaded porous silica supports				
MS-1	227.6	1.499	29.86	-
MS-2	111.5	1.531	54.91	-
BS-1	1,433	3.028	8.31	-
BS-2	412.1	1.497	14.53	-
Loaded porous silica supports				
Ni/MS-1	149.9	1.492	39.82	10.82
Ni/MS-2	90.26	1.219	54.02	13.50
Ni/BS-1	621.0	1.290	8.14	11.64
Ni/BS-2	359.3	1.260	14.03	14.68

X-ray diffraction (XRD) technique was used to investigate types and crystallite diameter of nickel oxide loaded on monomodal and bimodal porous silica supports. As shown in Figure 29, the catalysts consisted of NiO phase only which located at the 2θ of 37, 43 and 62°. Moreover, NiO crystallite diameters were calculated by using Scherer's equation as shown in Table 3. The crystallite diameters of both nickel loaded on monomodal and bimodal porous silica supports were closed

to each other. It could be explained that the diameters of nickel particles did not depend on total pore volume due to the fact that the small amount of nickel could stay separately and was not agglomerate with each other, leading to the similar nickel particle diameter on both of the monomodal and bimodal porous silica supports.

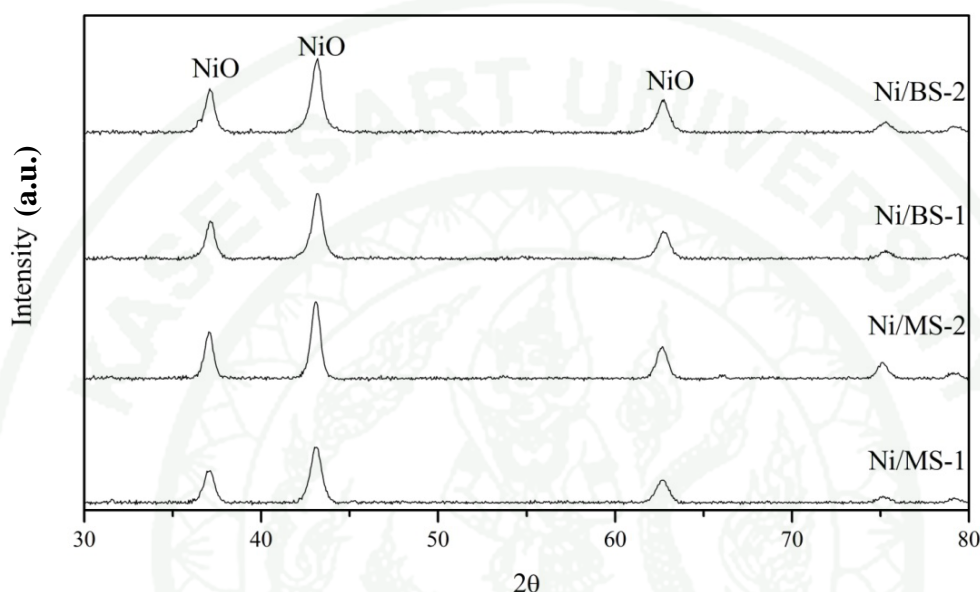


Figure 29 XRD patterns of nickel supported on various monomodal and bimodal porous silica supports.

The catalytic performances of nickel supported on monomodal and bimodal porous silica catalysts were tested for methane cracking reaction (MCR). The catalyst of 0.5 g was mixed with 2 g of sand to prevent the pressure build up and the temperature variation in the reactor. The obtained catalyst was packed in the inconel tube reactor and placed in the tube furnace. The reaction was performed under the conditions of atmospheric pressure and temperature of 500, 550, 600 and 650°C. The outlet gases were analyzed by using gas chromatography equipped with thermal conductivity detector (TCD) while the used catalysts and solid carbon nanotube products were examined by using thermogravimetric analysis (TGA) technique. CH₄ conversion and H₂ yield of nickel supported on monomodal and bimodal porous silica supports were shown in Figures 30 - 33.

In the case of Ni/MS-1 catalyst, CH₄ conversion and H₂ yield were shown in Figure 30(a) and (b), respectively. The highest CH₄ conversion and H₂ yield of Ni/MS-1 catalyst were obtained from the operating temperature of 500°C. Moreover, for Ni/MS-2 catalyst (Figure 31(a) and (b)), the maximum catalytic activity was found when the reaction was performed at the operating temperature of 550°C. It should be noted that the optimum operating temperature for methane cracking reaction was in the range of 500 - 550°C. At this temperature range, the rate of carbon nucleation was in equilibrium with the rate of surface carbon diffusion through nickel particle and the rate of carbon precipitation. Furthermore, the carbon nanotube products could encapsulate the nickel particle when the reaction was performed under the operating temperature beyond 550°C (Zhang and Amiridis, 1998). As a result, nickel supported on monomodal porous silica supports would exhibit higher CH₄ conversion and H₂ yield at low temperatures (500 and 550°C) than those of at high temperatures (600 and 650°C).

Furthermore, Ni/MS-1 catalyst showed the higher CH₄ conversions and H₂ yield for all operating temperatures than those of Ni/MS-2. It could be suggested that the larger total pore volume of interconnected channel structures (Figures 38(c) and (d)) and larger average pore diameter (Table 3) of Ni/MS-2 catalyst could provide faster carbon nanotubes (CNTs) formation than those of the smaller total pore volume and average pore diameter (Table 3) of Ni/MS-1 catalyst. Moreover, CNTs produced from methane cracking reaction over Ni/MS-2 catalyst could interrupt with other CNTs (Tsoncheva *et al.*, 2006), leading to the deactivation of nickel metal in Ni/MS-2 catalyst. Therefore, lower CH₄ conversion and H₂ yield were obtained when compared to those of Ni/MS-1 catalyst.

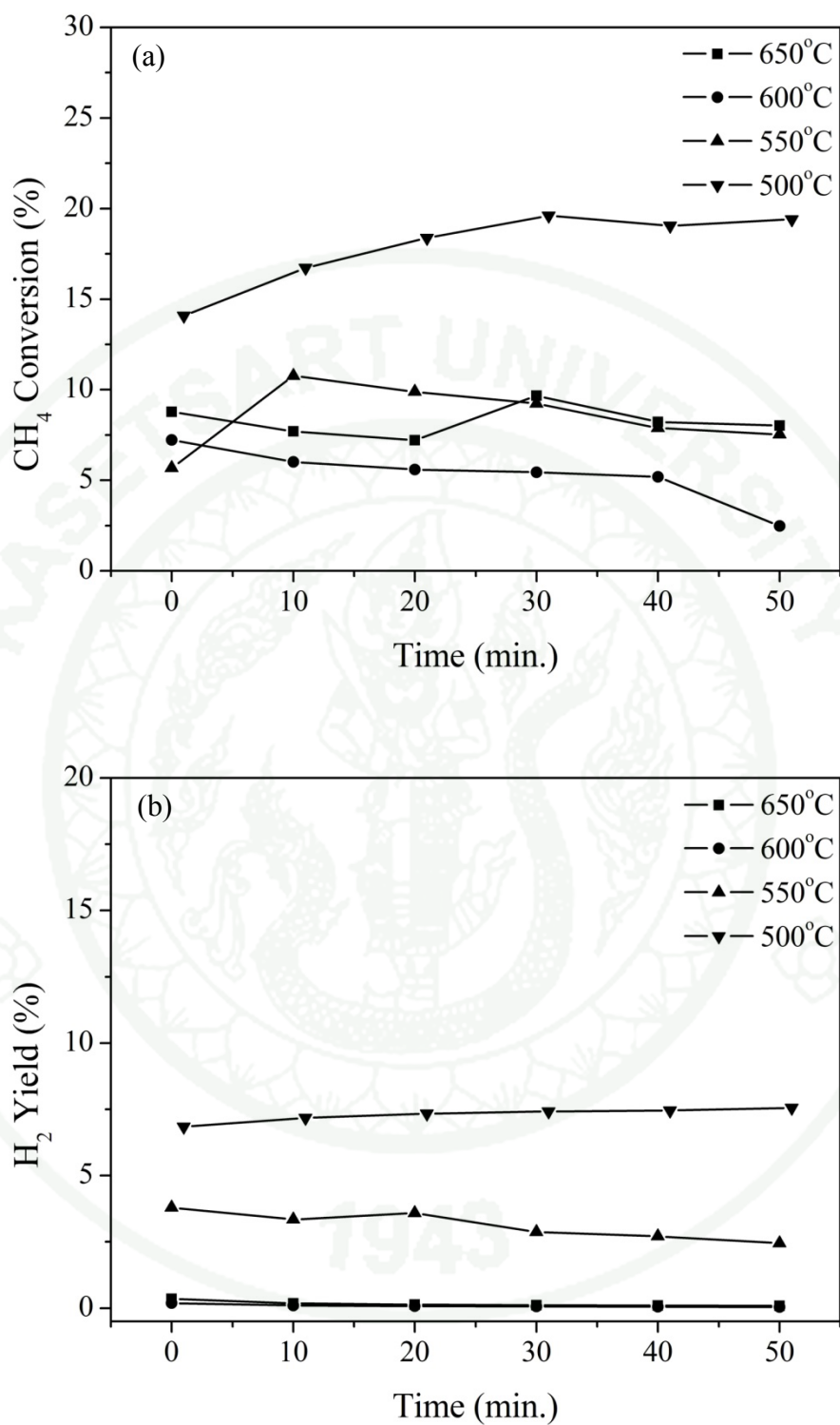


Figure 30 Catalytic activities of Ni/MS-1 catalyst (a) CH₄ conversion and (b) H₂ yield.

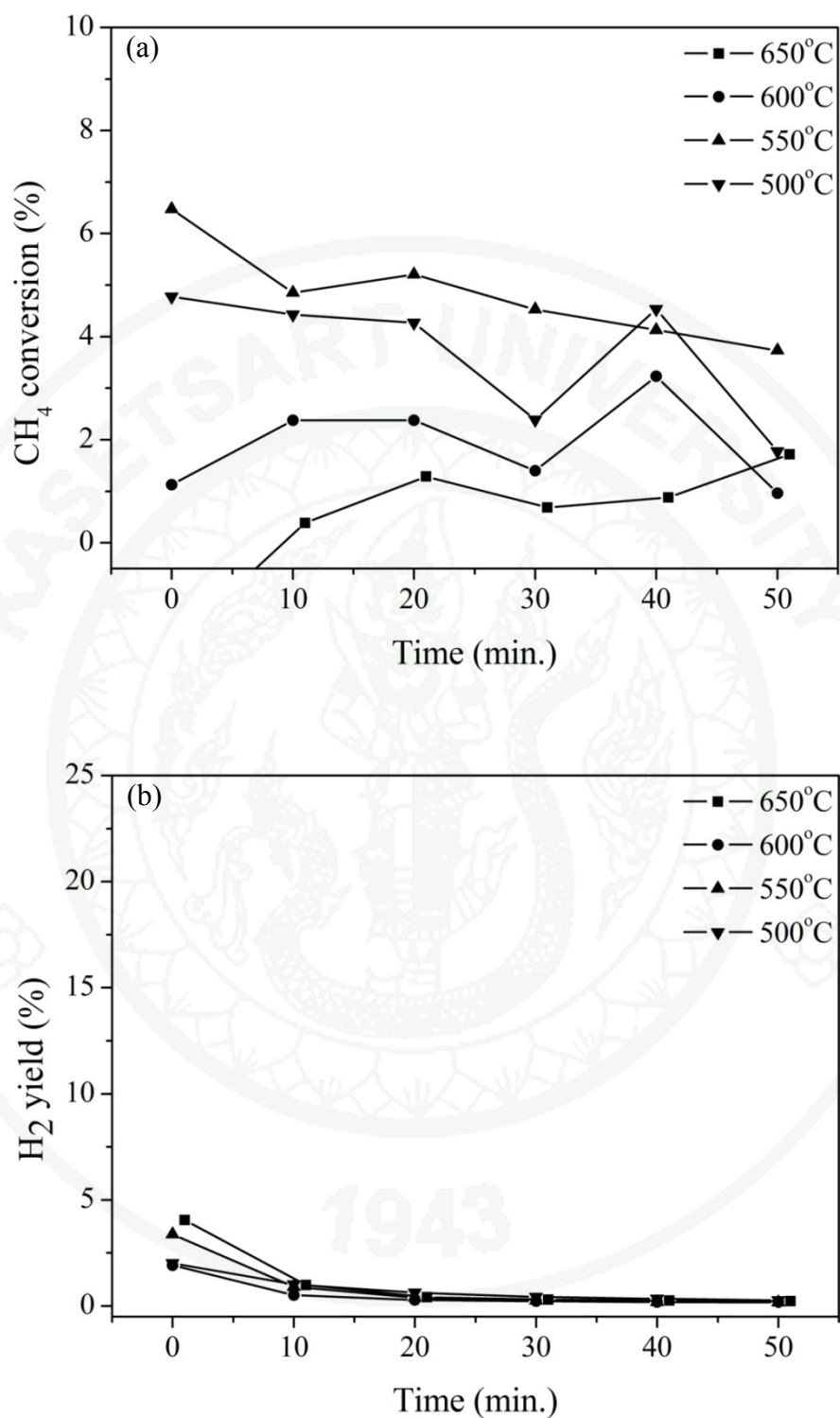


Figure 31 Catalytic activities of Ni/MS-2 catalyst (a) CH₄ conversion and (b) H₂ yield.

In the case of Ni/BS-1 catalyst (Figures 32(a) and (b)), CH₄ conversion and H₂ yield remained high after the methane cracking reaction was performed for 1 h, indicating that nickel supported on bimodal porous silica supports had higher stability when compared with those of nickel supported on monomodal porous silica supports. Moreover, CH₄ conversion and H₂ yield increased with the increasing in operating temperature and maximum at the operating temperature of 650°C while the lowest performance was observed at the temperature of 500°C. However, the CH₄ conversion and H₂ yield of Ni/BS-1 were higher than those of nickel supported on monomodal porous silica supports for all operating temperatures. It could be proposed that the carbon nanotube products might not encapsulate the nickel particle deposited on BS-1 support, therefore nickel particles were still active at high operating temperature. In this case, it was clearly seen that the growth of carbon nanotubes depended on the operating temperature. For Ni/BS-2 (Figure 33(a) and (b)), similar trends of CH₄ conversion and H₂ yield were observed. Moreover, Ni/BS-2 showed the higher CH₄ conversion and H₂ yield than those of Ni/BS-1 which in agreement with Venugopol *et al.* (2008) who used Ni/SiO₂ to investigate the effect of nickel particle size on the catalytic activity of methane cracking reaction. They found that the larger nickel particle size gave the better CH₄ conversion. Therefore, Ni/BS-2 catalyst which contained the larger nickel particle size could give the higher CH₄ conversion and H₂ yield compared to those of Ni/BS-1 catalyst.

Furthermore, the nickel supported on bimodal porous silica supports exhibited the higher CH₄ conversion and H₂ yield when compared to those of nickel supported on monomodal porous silica supports. This could be attributed to the fact that the large total pore volume of monomodal porous silica supports provided the fast growth rate of CNTs from methane cracking reaction. The fast growth rate of CNTs provided the long length of CNTs. However, nickel particle detached from monomodal porous silica supports by CNT could be deactivated by the encapsulation of other CNTs formed on neighbor nickel particles (Tsoncheva *et al.*, 2006). Due to the fast formation rate of CNTs, the fast deactivation rate of nickel particle would be obtained. Therefore, nickel supported on monomodal porous silica supports would

show the lower CH_4 conversion and H_2 yield than those of nickel supported on bimodal porous silica supports.

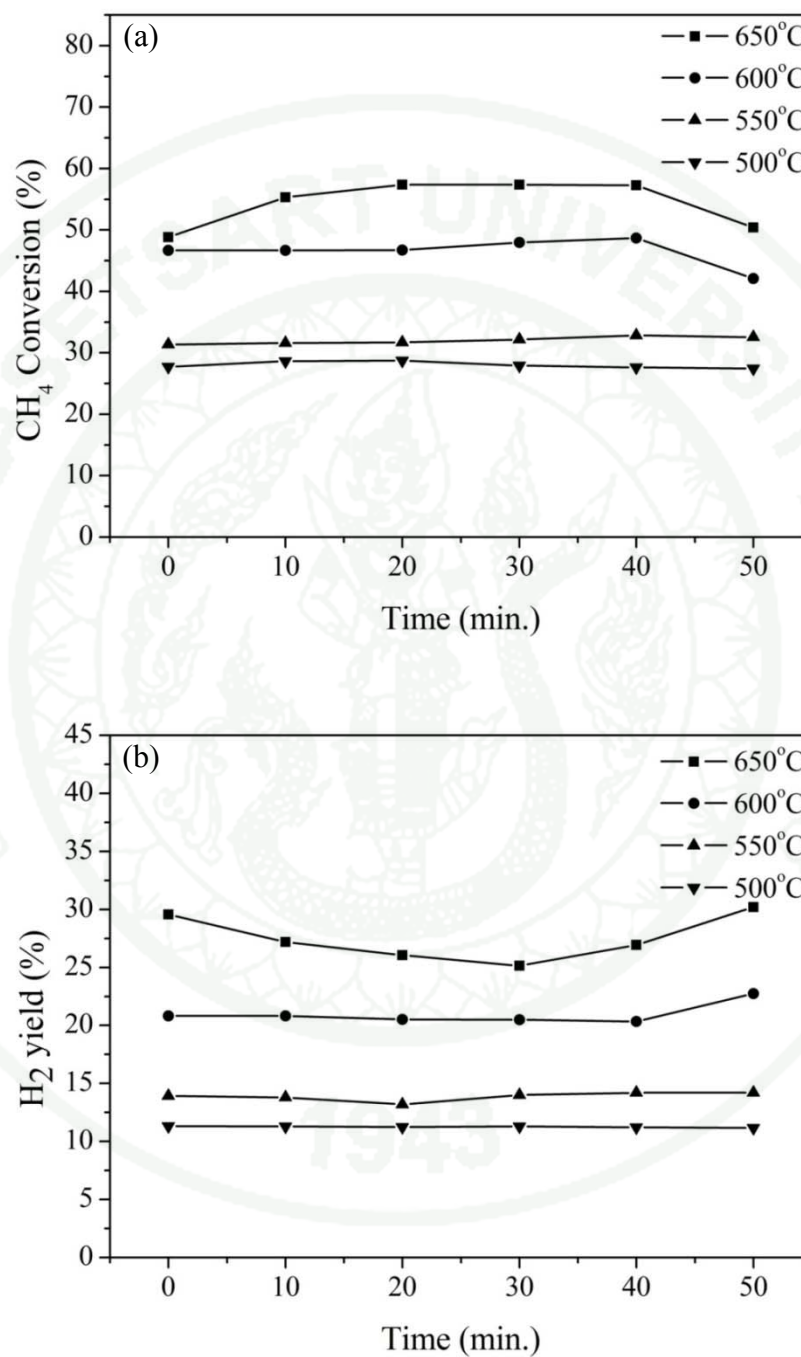


Figure 32 Catalytic activities of Ni/BS-1 catalyst (a) CH_4 conversion and (b) H_2 yield.

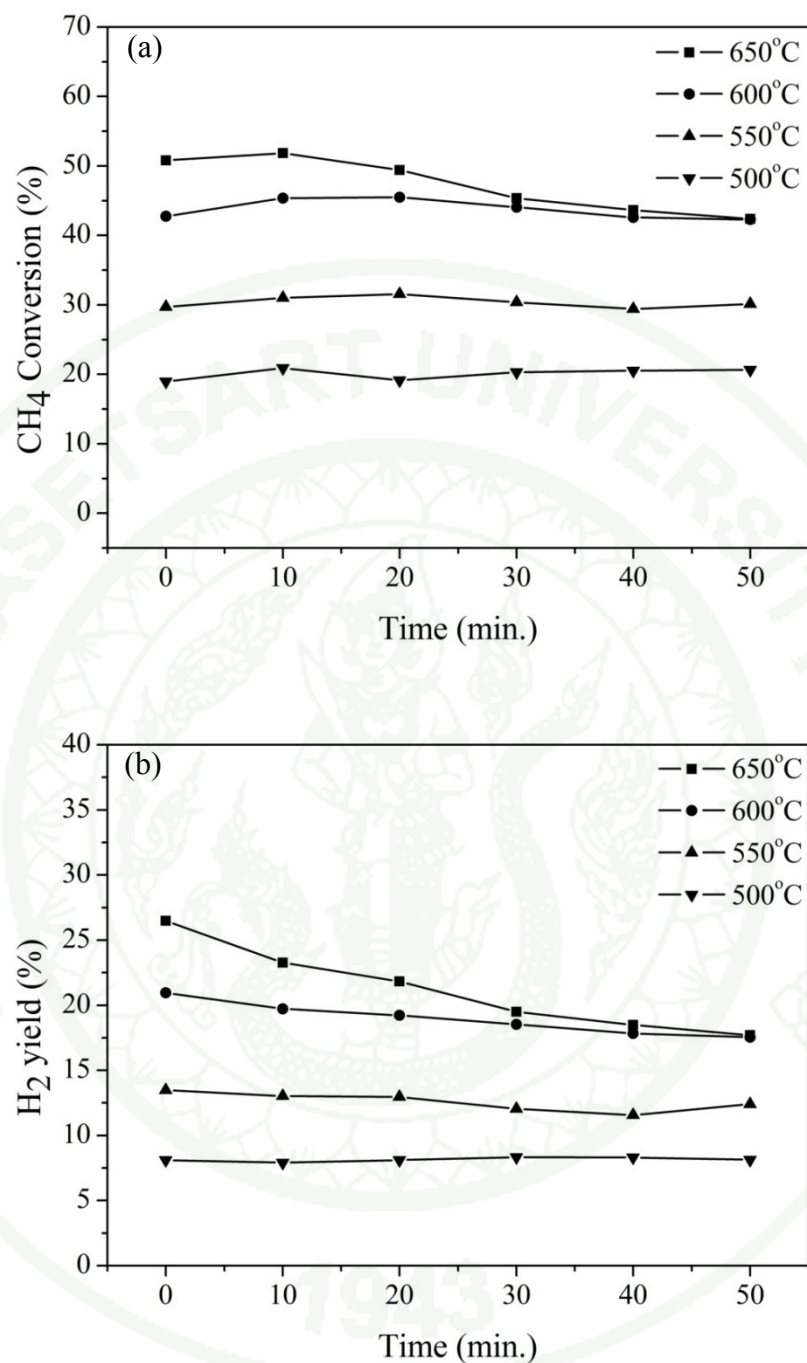


Figure 33 Catalytic activities of Ni/BS-2 catalyst (a) CH₄ conversion and (b) H₂ yield.

Thermogravimetric analysis (TGA) technique was used to investigate the amount and types of the product carbon species. TGA and differential thermal analysis (DTA) of Ni/MS-1 and Ni/MS-2 operated at 500, 550, 600 and 650°C are

shown in Figures 34(a) and (b). It was found that TGA of Ni/MS-1 catalysts exhibited two steps weight losses. The first weight loss was below than 150°C, representing the evaporation of adsorbed water in the pores of catalysts. The second weight loss located at 430°C was the combustion of single-wall carbon nanotubes (SWCNTs) which in good agreement with Mansfield *et al.* (2010). In the case of Ni/MS-2 catalyst (Figures 35(a) and (b)), TGA results showed three steps of weight losses. Similar to those of Ni/MS-1 catalyst, the first and second of weight losses were the evaporation of water trapped in the pores of MS-2 support and the combustion of SWCNTs produced by methane cracking reaction over Ni/MS-2 catalyst, respectively. The third step located at 850°C was the combustion of multi-wall carbon nanotubes (MWCNTs) which in agreement with Vicente *et al.* (2011). Moreover, weight loss percentages of Ni/MS-2 of all operating temperatures were lower than those of Ni/MS-1 catalyst. It should be explained that the large total pore volume and average pore diameter of Ni/MS-2 catalyst could exhibit the fast formation rate of CNTs during methane cracking reaction. The produced CNTs were obstructed by neighboring CNTs, leading to the deactivation of nickel metals (Tsoncheva *et al.*, 2006). Therefore, CH₄ conversion, H₂ yield and the amount of CNTs product over Ni/MS-2 catalyst were lower than those of Ni/MS-1 catalyst.

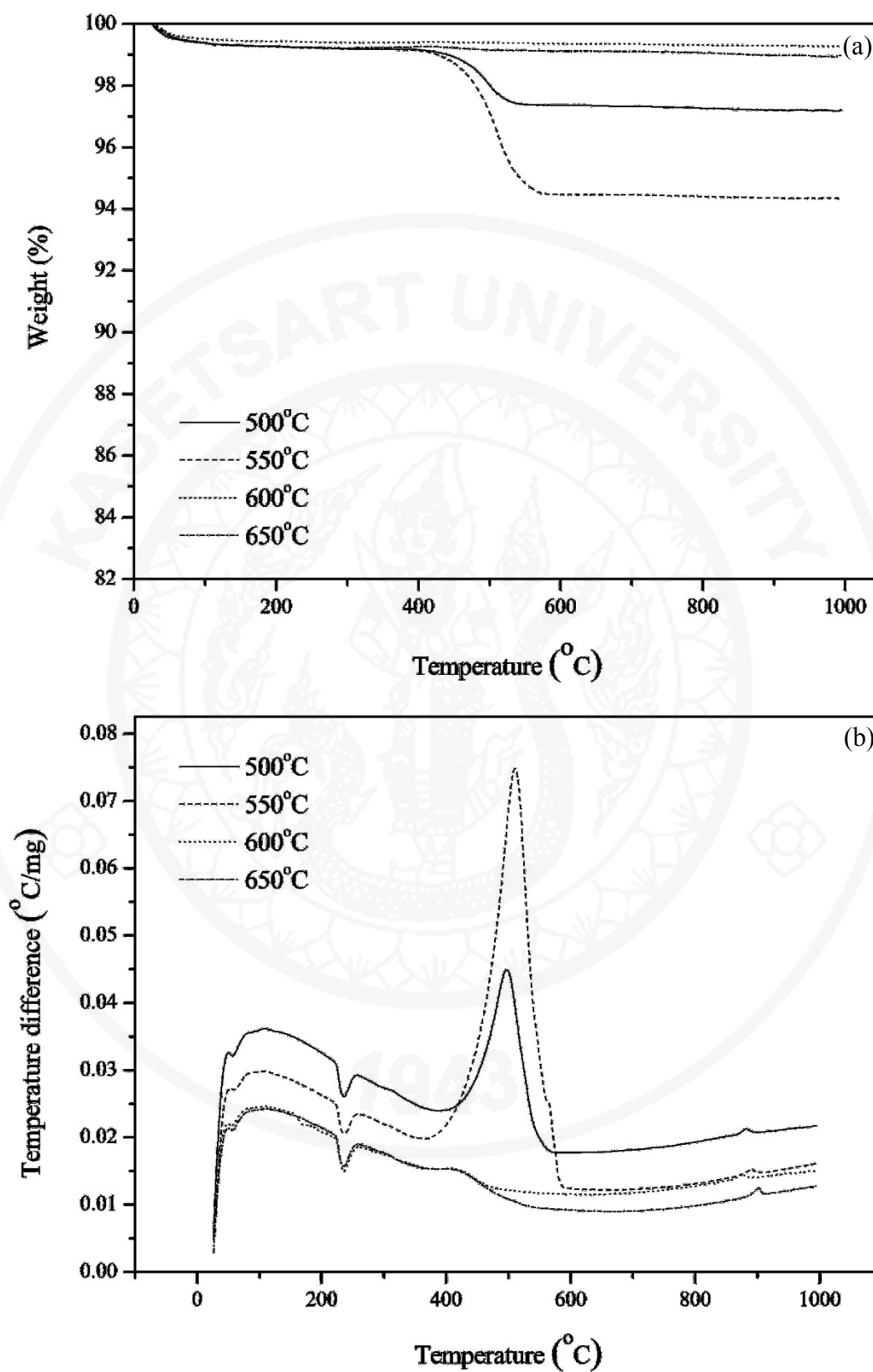


Figure 34 (a) TGA and (b) DTA of Ni/MS-1 catalyst.

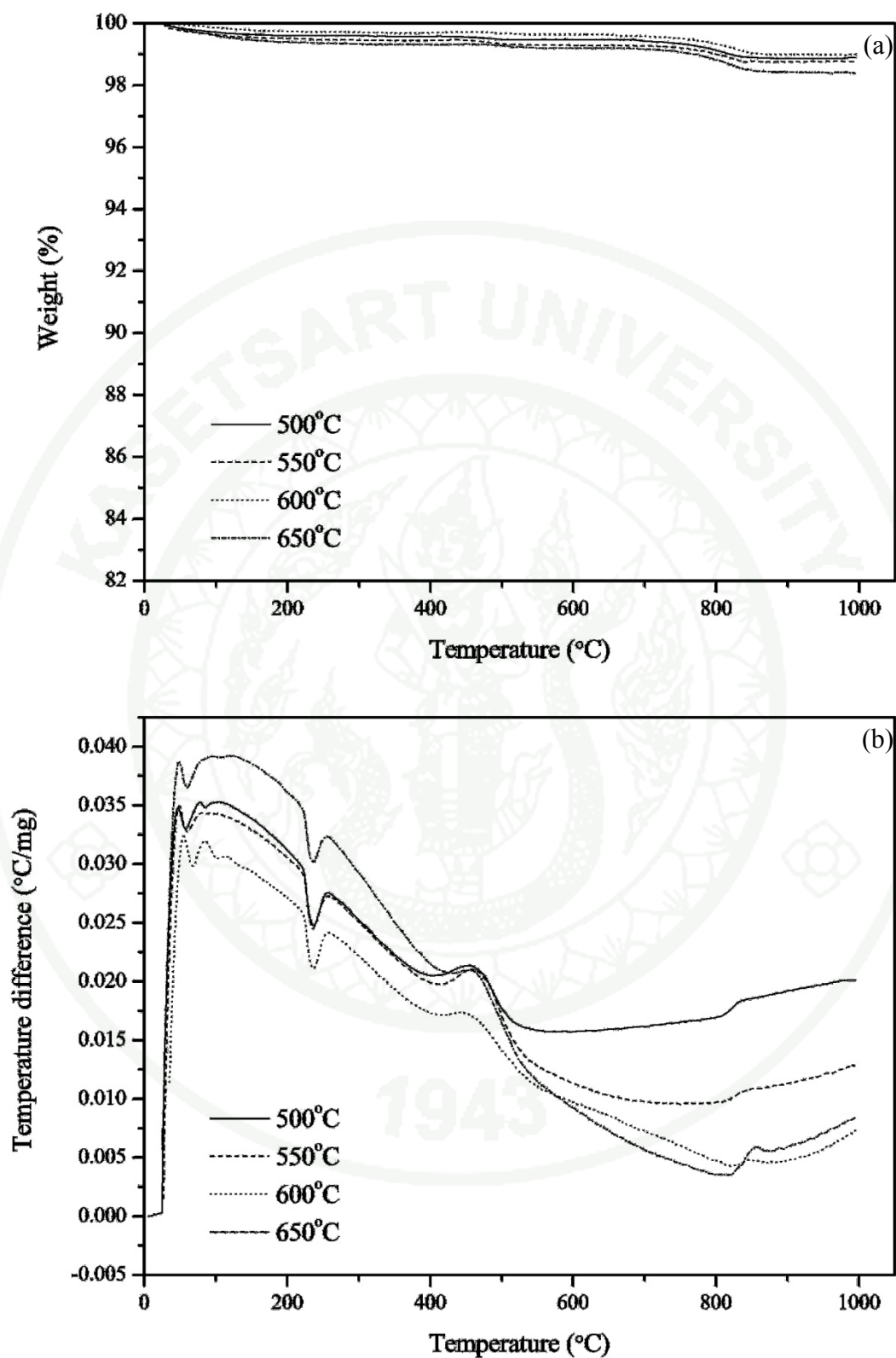


Figure 35 (a) TGA and (b) DTA of Ni/MS-2 catalyst.

In the case of nickel supports on bimodal porous silica supports (Figures 36(a) and (b) for Ni/BS-1 and Figures 37(a) and (b) for Ni/BS-2 catalysts), the catalysts exhibited two steps of weight losses. The first step occurred at temperature below 150°C was the evaporation of water molecules trapped in the catalyst pores. The second weight loss, which occurred at temperature beyond 150°C, was the combustion of SWCNTs products as was confirmed by exothermic peaks shown in Figures 36(b) and 37(b). Moreover, the maximum weight losses of nickel supported on bimodal porous silica supports were obtained from the catalysts performed the MCR at temperature of 650°C. It could be explained that the maximum CH₄ conversion was found at this temperature, leading to the highest amount of methane converted to hydrogen and carbon nanotube products. On the other hand, the lowest weight losses were observed from the catalysts performed methane cracking reaction at the operating temperature of 500°C for both of Ni/BS-1 and Ni/BS-2 catalysts.

Furthermore, nickel supported on bimodal porous silica supports exhibited the higher weight losses than those of nickel supported on monomodal porous silica supports, indicating that Ni/BS-1 and Ni/BS-2 could promote the higher amount of carbon nanotube formation than those of Ni/MS-1 and Ni/MS-2. It should be explained that the structure of interconnected channel structures of monomodal porous silica supports were inappropriate to methane cracking reaction. This was because the large pore of interconnected channel provided the fast growth rate of CNTs than those of bimodal porous silica supports. Nickel particles detached from monomodal porous silica supports were deactivated by other CNT formed on neighbor nickel particle (Tsoncheva *et al.*, 2006). As mentioned before, the fast formation rate of CNTs could cause the fast deactivation rate of nickel particles. Therefore, the lower deactivation of nickel particle would be observed from nickel supported on bimodal porous silica supports compared to those of nickel supported on monomodal porous silica supports, leading to the lower amount of CNTs would be found in nickel supported on monomodal porous silica supports.

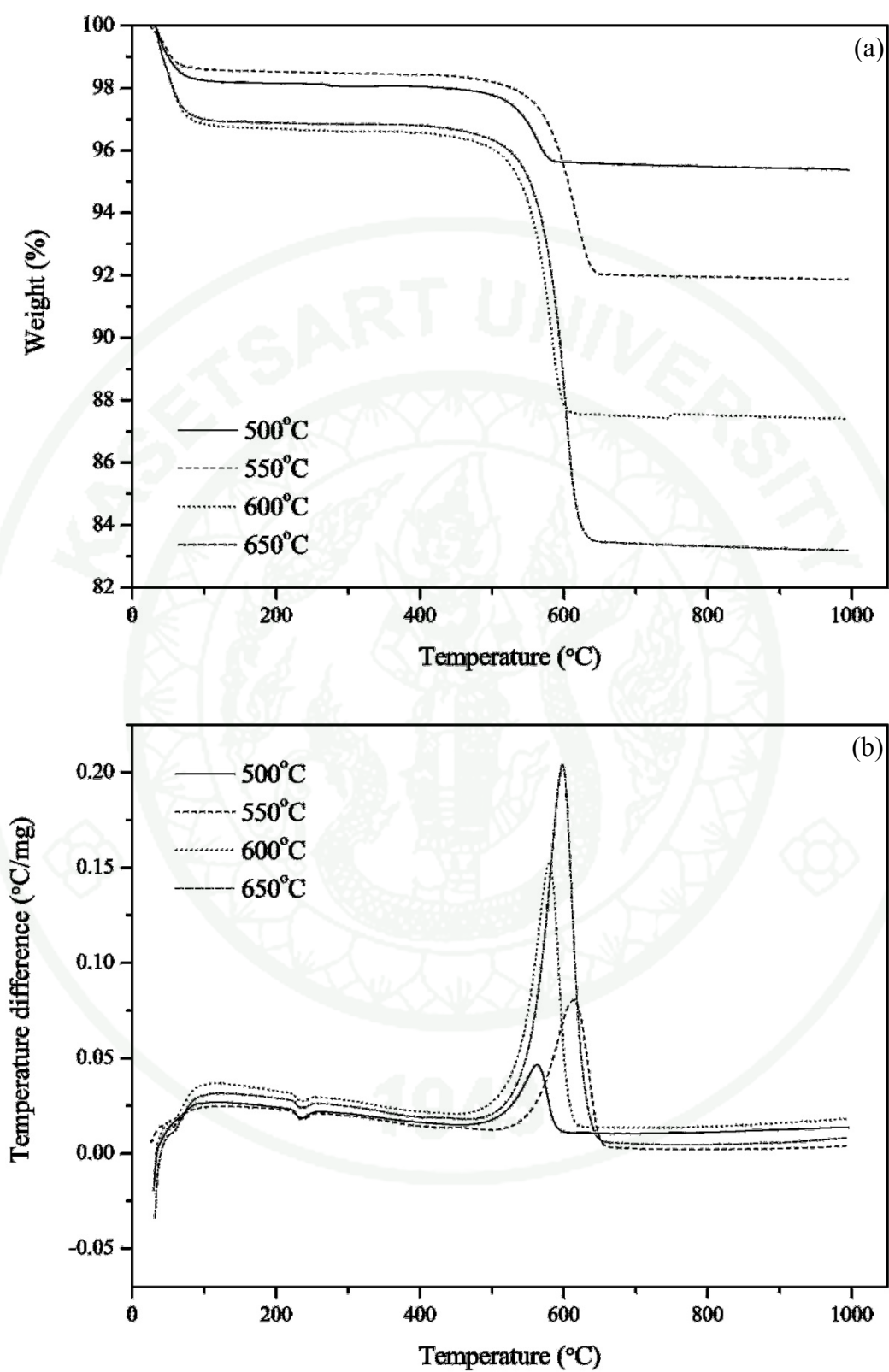


Figure 36 (a) TGA and (b) DTA of Ni/BS-1 catalyst.

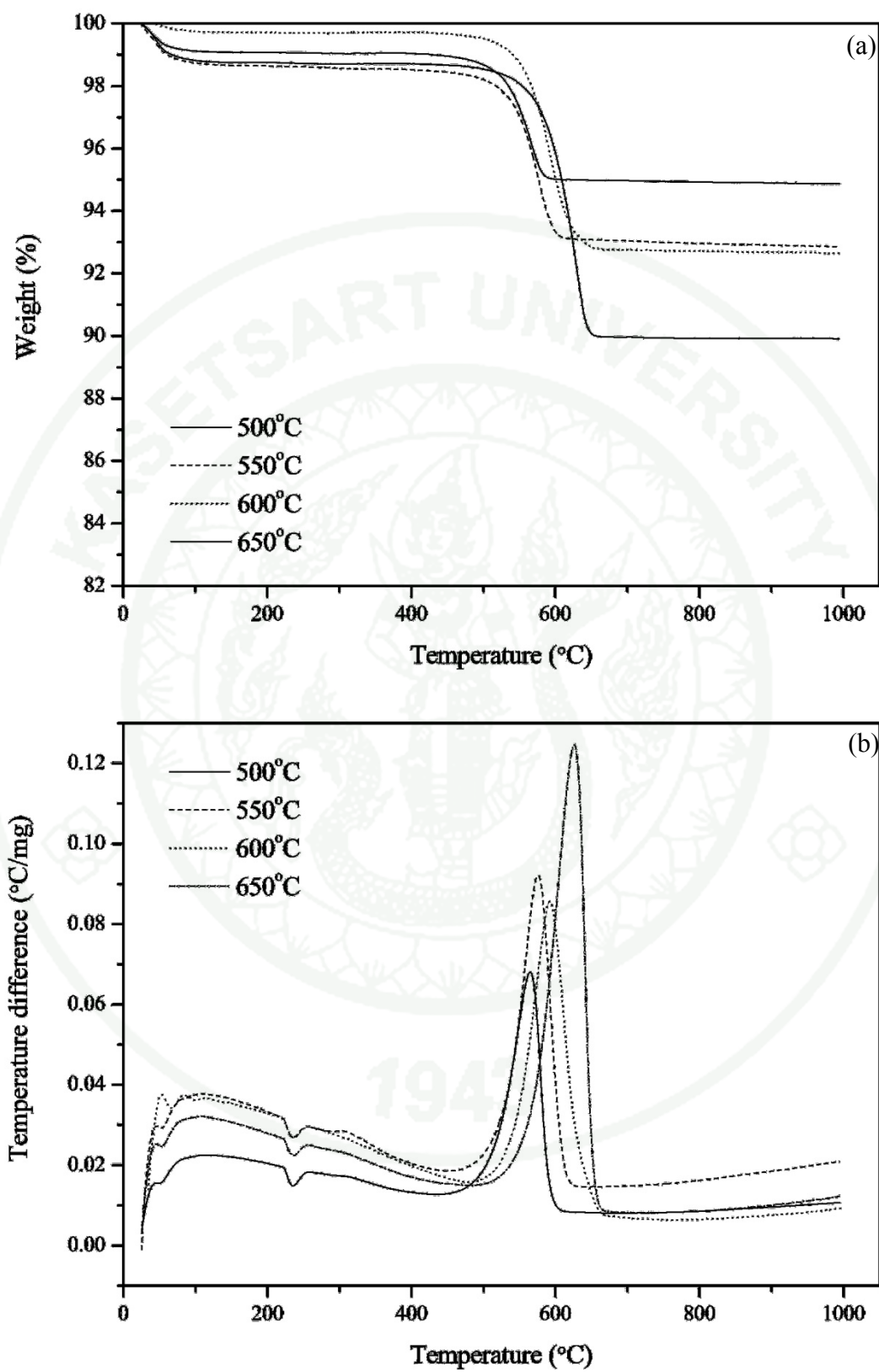


Figure 37 (a) TGA and (b) DTA of Ni/BS-2 catalyst.

In order to investigate types and approximate amount of CNTs which were produced from methane cracking reaction, Scanning Electron Microscope (SEM) was applied. SEM images of the used Ni/MS-1 and Ni/MS-2 catalysts were shown in Figures 38 and 39, respectively. The interconnected xerogel structures were observed in all the monomodal porous silica supports. However, the higher total pore volume and larger diameter of silica nanoparticles were observed with Ni/MS-2 catalyst when compared to those of Ni/MS-1 catalyst due to the effect of pH values. It should be noted that small amount of CNTs produced from MCR over nickel supported on monomodal porous silica supports were observed at the operating temperature of 600 and 650°C. On the other hand, the higher amount of CNTs were found at low operating temperatures (500 and 550°C) as shown in Figures 38(a) and (b) and Figures 39(a) and (b) for Ni/MS-1 and Ni/MS-2 catalyst, respectively. The long length CNTs were formed on nickel particles which loaded on monomodal porous silica supports. At high CH₄ conversion, high amounts of methane gas were decomposed to form hydrogen and carbon products. Carbon atoms could possibly deposit on the air-nickel interface and diffuse through nickel particle to nickel-support interface. At nickel-support interface, carbon began to form the carbon nanotubes (Snoeck *et al.*, 1997). Moreover, the amount of produced CNTs from methane cracking reaction over Ni/MS-2 catalyst was lower than those of Ni/MS-1 catalyst. It should be explained that the CNTs growth rate in large total pore volume and large average pore diameter of Ni/MS-2 catalyst was faster than that of small total pore volume and narrow average pore diameter of Ni/MS-1 catalyst which in agreement with Tsoncheva *et al.* (2006). Moreover, CNTs produced from methane cracking reaction over Ni/MS-2 catalyst could be disturbed by other CNTs, causing the deactivation of nickel particles detached from monomodal porous silica supports by CNT (Tsoncheva *et al.*, 2006). As nickel particles were deactivated, CH₄ conversion and H₂ yield of nickel supported on monomodal porous silica supports should lower than those of nickel supported on bimodal porous silica supports, leading to the lower amount of CNTs was formed on nickel supported on monomodal porous silica supports compared to those of nickel supported on bimodal porous silica supports.

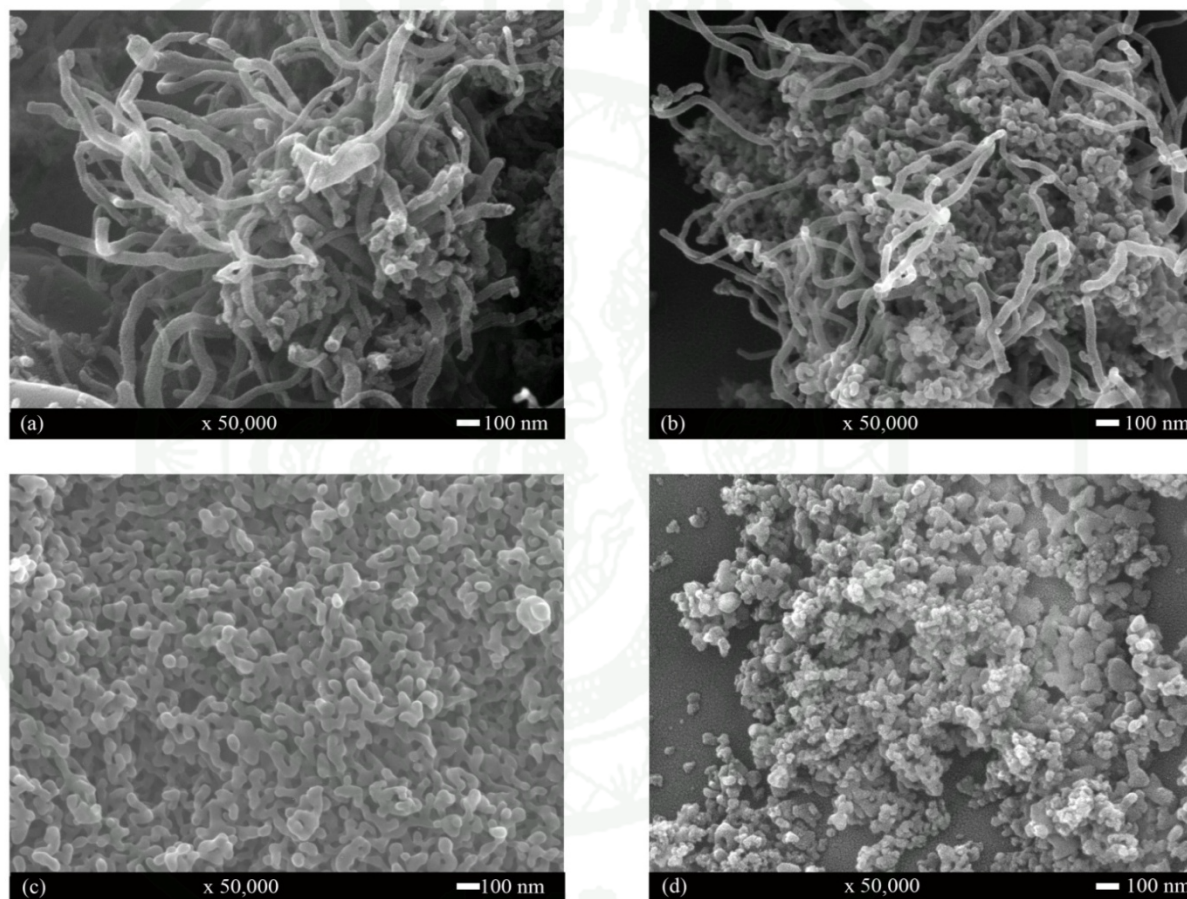


Figure 38 SEM images of Ni/MS-1 performed methane cracking reaction at (a) 500°C, (b) 550°C, (c) 600°C and (d) 650°C.

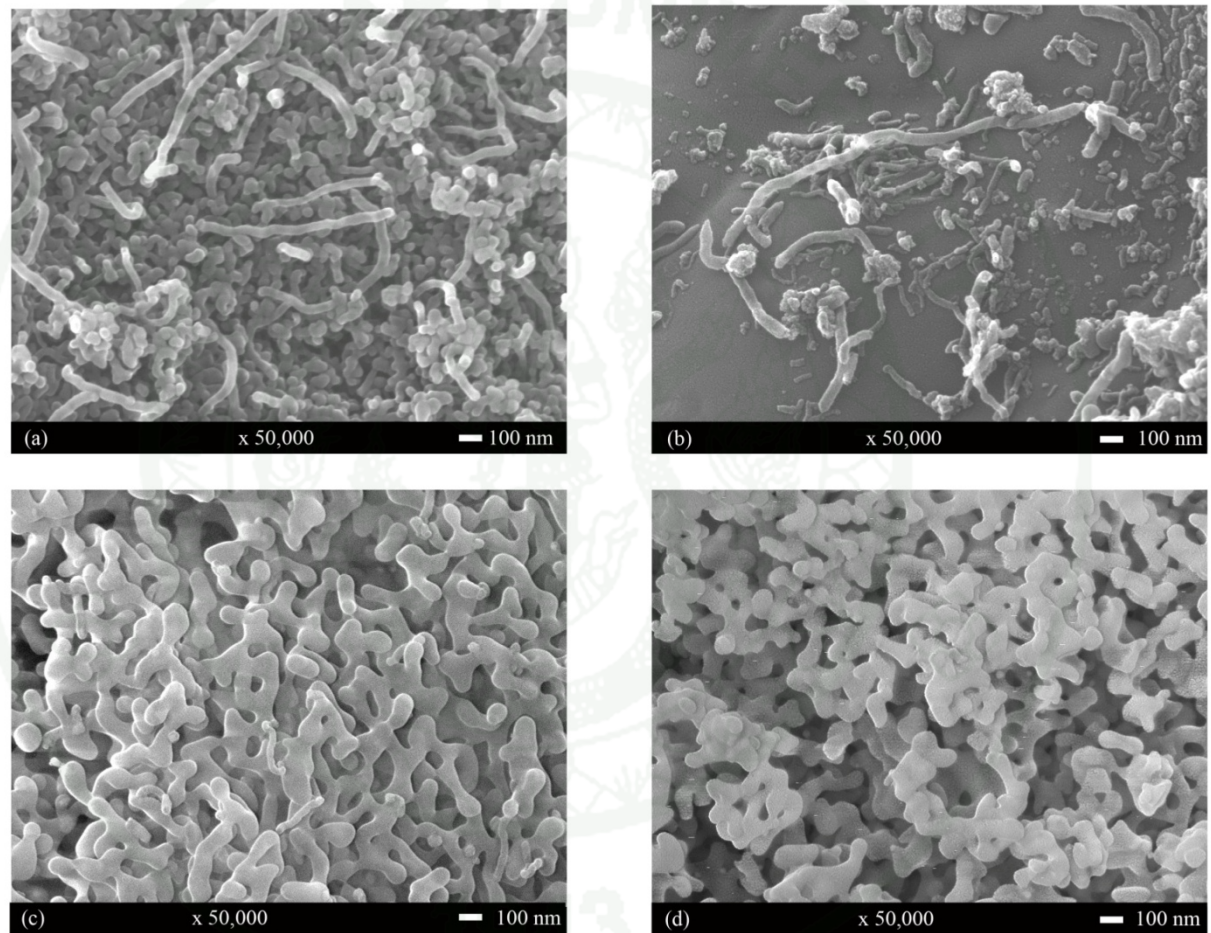


Figure 39 SEM images of Ni/MS-2 performed methane cracking reaction at (a) 500°C, (b) 550°C, (c) 600°C and (d) 650°C.

The SEM images of Ni/BS-1 and Ni/BS-2 catalysts are shown in Figures 40 and 41, respectively. Carbon nanotubes were observed in both catalysts operated at all operating temperatures. In this series of experiment, the highest amount of carbon nanotubes was obtained at the operating temperature of 650°C for both Ni/BS-1 and Ni/BS-2 catalysts because at this temperature the maximum CH₄ conversions were occurred. However, Ni/BS-2 catalyst showed the higher amount of carbon nanotubes than that of Ni/BS-1 catalyst because Ni/BS-2 catalyst exhibited the higher CH₄ conversion. Moreover, the amount of carbon nanotubes produced from nickel supported on bimodal porous silica supports were higher than nickel supported on monomodal porous silica supports.

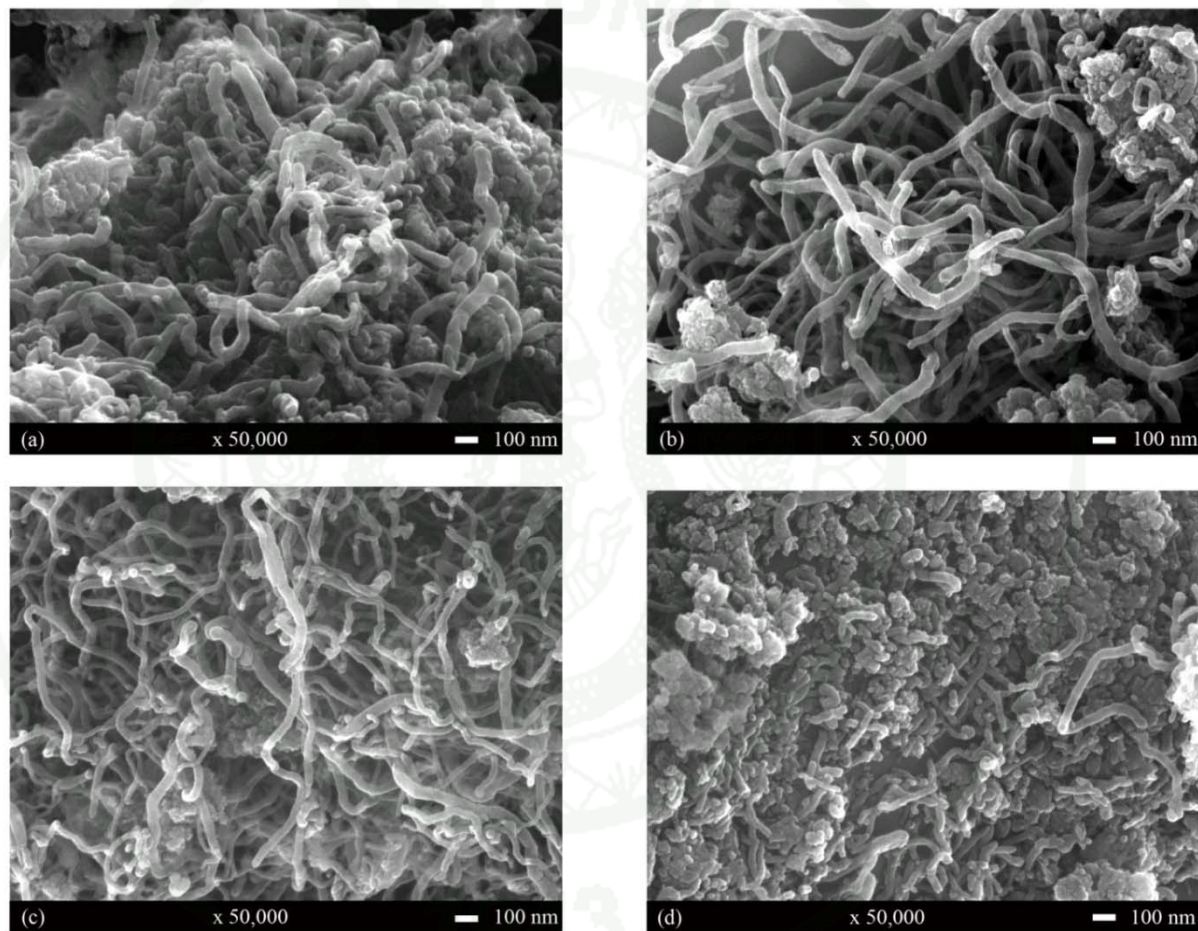


Figure 40 SEM images of Ni/BS-1 performed methane cracking reaction at (a) 500°C, (b) 550°C, (c) 600°C and (d) 650°C.

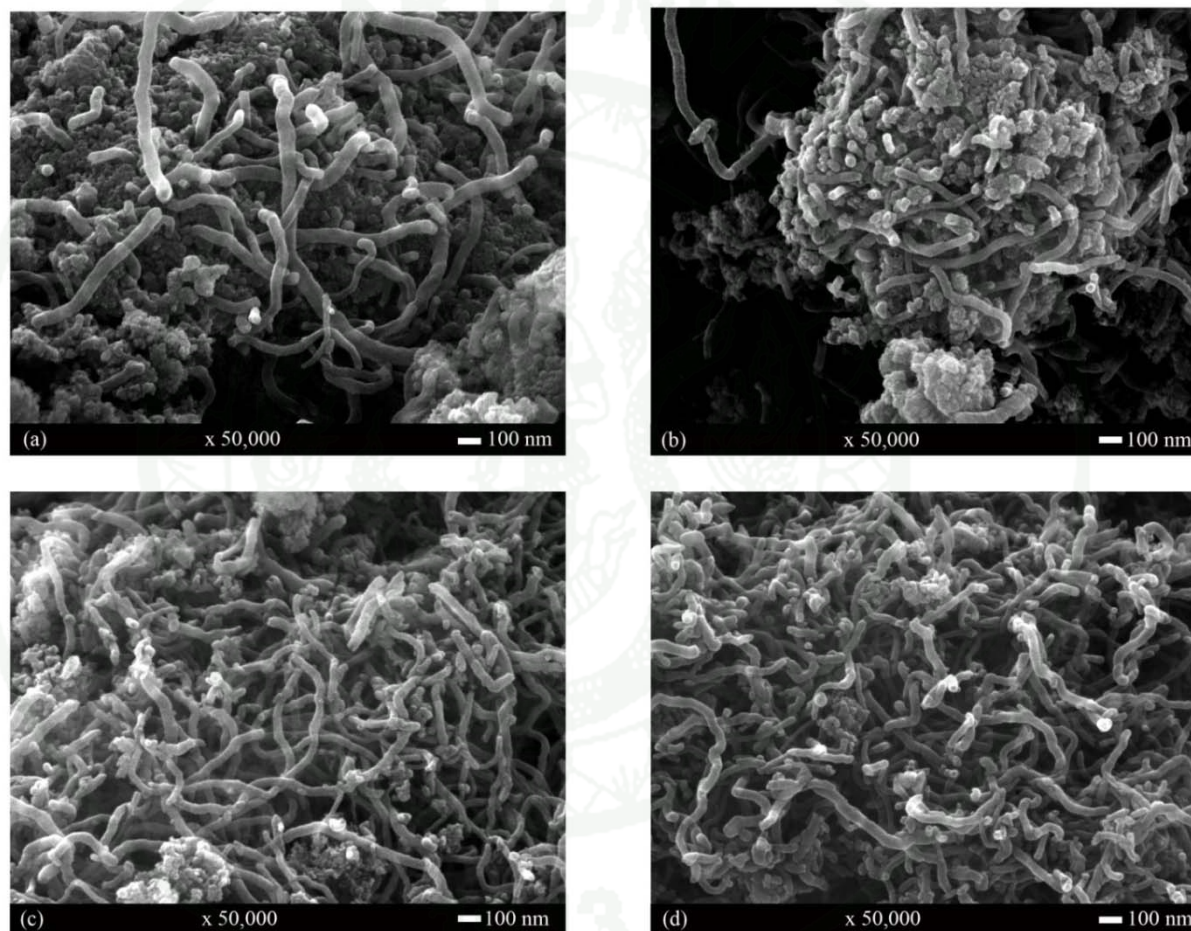


Figure 41 SEM images of Ni/BS-2 performed methane cracking reaction at (a) 500°C, (b) 550°C, (c) 600°C and (d) 650°C.

As mentioned before, CH₄ conversion and H₂ yield were affected from operating temperatures. In order to understand more clearly regarding the effect of temperature, the activation energies of methane cracking over nickel supported on monomodal and bimodal porous silica supports were examined as shown in Figures 42(a) and (b), respectively. Moreover, the activation energies of methane cracking over catalysts were estimated by using an Arrhenius plot of $\ln k$ against $1/T$ in which the gradient was $-E_a/R$. The activation energies were summarized in Table 4. The Arrhenius plot of Ni/MS-1 and Ni/MS-2 exhibited the positive gradient, indicating that E_a of the catalysts were negative values. On the other hand, the negative gradients of Arrhenius plot were observed from both Ni/BS-1 and Ni/BS-2 catalysts. Therefore, E_a of nickel supported on bimodal porous silica supports would be of positive values. Actually, the activation energy could not be zero or negative values since it would violate the Arrhenius law. However, the negative activation energy had been reported for the reaction that was independent with temperature (Mozurkewich and Sidney, 1984 and Bai *et al.*, 2005). Therefore, methane cracking reaction over nickel supported on monomodal porous silica supports would not depend on temperature. As mention before, the encapsulation of nickel particle by carbon nanotubes was occurred at high operating temperature which in agreement with negative activation energies.

In the case of nickel supported on bimodal porous silica supports, the positive activation energies were obtained. The activation energies of Ni/BS-1 and Ni/BS-2 were 41.22 and 32.61 KJ/mol, respectively, which lower than that of Bai *et al.* (2005) who used activated carbon as the catalyst for methane decomposition reaction. They found the activation energies of methane decomposition reaction over activated carbon were in the range of 117 – 185 KJ/mol. The less activation energies implied that the reaction rate was less sensitive to temperature (Bai *et al.*, 2006), causing the Arrhenius plot of both Ni/BS-1 and Ni/BS-2 catalysts were closed with each other. Therefore, CH₄ conversion and H₂ yield of Ni/BS-1 and Ni/BS-2 were slightly differences.

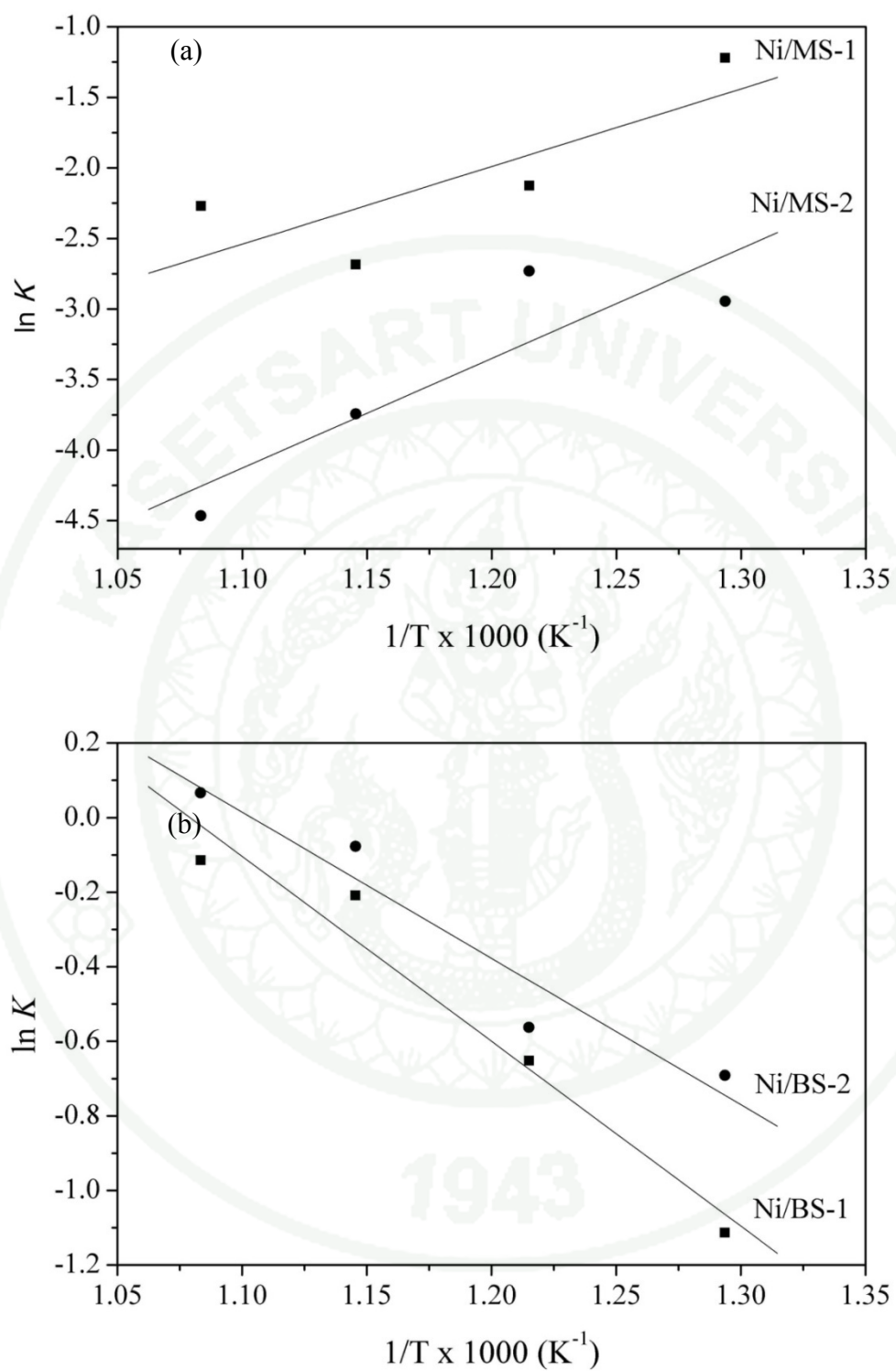


Figure 42 Arrhenius plot of nickel supported on (a) monomodal and (b) bimodal porous silica supports.

Table 4 Activation energy of nickel loaded on monomodal and bimodal porous silica supports

Catalysts	Ea (KJ/mol)*
Nickel loaded on monomodal porous silica supports	
Ni/MS-1	- 45.72
Ni/MS-2	- 64.65
Nickel loaded on bimodal porous silica supports	
Ni/BS-1	41.22
Ni/BS-2	32.61

* calculated from the gradient of Arrhenius plot.

CONSLUSION

In this research, the effect of different two pore sizes of bimodal porous silica supports on methane cracking reaction was investigated. The studied variables were the structure of porous silica support including monomodal and bimodal porous silica support and operating temperature of methane cracking reaction. The results were summarized as follows:

1. CH_4 conversion and H_2 yield were increased with increasing of mean pore diameter for nickel supported on bimodal porous silica supports while nickel supported on monomodal porous silica supports exhibited the decreasing of CH_4 conversion and H_2 yield as the mean pore diameters were increased. Moreover, CH_4 conversions and H_2 yields of nickel supported on bimodal porous silica supports exhibited higher than those of nickel supported on monomodal porous silica supports. As a result, macroporosity of catalysts supports greatly affected the methane cracking reaction.

2. In the case of nickel supported on monomodal porous silica supports, methane cracking reaction was independent with operating temperature as the negative activation energies were obtained. At lower operating temperature (500 and 550°C), the higher CH_4 conversion and H_2 yield were observed when compared to those of higher operating temperature (600 and 650°C). For nickel supported on bimodal porous silica supports, methane cracking reaction was slightly affected by operating temperature due to the less activation energies. The higher operating temperature, the higher CH_4 conversion and H_2 yield would be observed.

LITERATURE CITED

- Aiello, R., Fiscus J.E., zurLoye H.C. and Amiridis M.D. 2000. Hydrogen production via the direct cracking of methane over Ni/SiO₂: catalyst deactivation and regeneration. **Applied Catalysis A: General** 192: 227 - 234.
- Alstrup, I. 1988. A new model explaining carbon filament growth on nickel, iron, and Ni-Cu alloy catalysts. **Journal of Catalysis** 109: 241-251.
- Avdeeva, L.B., T.V. Reshetenko, Z.R. Ismagilov and V.A. Likholobov. 2002. Iron-containing catalysts of methane decomposition: accumulation of filamentous carbon. **Applied Catalysis A - General** 228: 53 - 63.
- Bai, Z., H. Chen, W. Li and B. Li. 2005. Catalytic decomposition of methane over activated carbon. **Journal Of Analytical And Applied Pyrolysis** 73: 335 – 341.
- _____, _____, _____ and _____. 2006. Hydrogen production by methane decomposition over coal char. **International Journal of Hydrogen Energy** 31: 899 – 905.
- Baker, R.T.K., M.A. Barber, P.S. Harris, F.S. Feates and R.J. Waite. 1972. Nucleation and growth of carbon deposits from the nickel catalyzed decomposition of acetylene. **Journal of Catalysis** 26: 51 - 62.
- Bartholomew, C.H. and J.F. Robert. 2005. Fundamentals of industrial catalytic processes. **Wiley-AIChE**. New Jersey.
- Brinker, C.J. and G.W. Scherer. 1990. SOL-GEL SCIENCE the Physics and Chemistry of Sol-Gel Processing. **Academic Press, Inc.** United Kingdom.

- Boellaard, E., P.K. de Bokx, A.J.H.M. Kock and J.W.Geus 1985. The formation of filamentous carbon on iron and nickel catalysts: III. Morphology. **Journal of Catalysis** 96: 481 - 490.
- Chareonpanich, M., T.Namto, P.Kongkachuichay, J.Limtrakul. 2004. Synthesis of ZSM-5 zeolite from lignite fly ash and rice husk ash. **Fuel Processing Technology** 85: 1623 - 1634.
- Chesnokov, V.V. and A.S. Chichkan. 2009. Production of hydrogen by methane catalytic decomposition over Ni-Cu-Fe/Al₂O₃ catalyst. **International Journal of Hydrogen Energy** 34: 2979 - 2985.
- Choudhary, H., T. Harvey, W. C. Thayer, T. F. Lockwood, W. M. Stiteler, P. E. Hassett J. M. Goodrum and G. L. Diamond. 2001. Urinary cadmium elimination as a biomarker of exposure for evaluating acadmium dietary exposure: biokinetics model. **Journal of Toxicology and Environmental** 63 (5): 321 – 350.
- Deutschmann, O. and L. D. Schmidt. 1998. Two-dimensional modeling of partial oxidation of methane on rhodium in a short contact time reactor. **Twenty-seventh Symposium (International) on Combustion. The Combustion institute**: 2283–2291.
- Echegoyen, Y., I. Suelves, M.J. La'zaro, R. Moliner and J.M. Palacios. 2007. Hydrogen production by thermo-catalytic decomposition of methane over Ni-Al and Ni-Cu-Al catalysts: effect of calcination temperature. **Journal of Power Sources** 169: 150 - 157.
- Ermakova, M.A., D.Y. Ermakov and G.G. Kuvshinov. 2000. Effective catalysts for direct cracking of methane to produce hydrogen and filamentous carbon: Part I. Nickel catalysts. **Applied Catalysis A – General** 201: 61 - 70.

- Ichioaka, H., N. Higashi, Y. Yamada, T. Miyake and T. Suzuk. 2007. Carbon nanotube and nanofiber syntheses by the decomposition of methane on group 8 -10 metal loaded MgO catalyst. **Diamond and Related Materials** 16: 1121 - 1125.
- Jullaphan, O., T. Witoon, M. Chareonpanich. 2009. Synthesis of mixed-phase uniformly infiltrated SBA-3-like in SBA-15 bimodal mesoporous silica from rice husk ash. **Materials Letters** 63: 1303–1306.
- Kock, A.J.H.M., P.K. de Bokx, E. Boellaard, W. Klop and J.W. Geus. 1985. The formation of filamentous carbon on iron and nickel catalysts: II. Mechanism. **Journal of Catalysis** 96: 468 - 480.
- Lázaro, M.J., Y. Echevoyena, C. Alegrea, I. Suelvesa, R. Molinera and J.M. Palacios. 2008. TiO₂ as textural promoter on high loaded Ni catalysts for methane decomposition. **International Journal of Hydrogen Energy** 33: 3320 – 3329.
- Mansfield, E., A. Kar and S.A. Hooker. 2010. Applications of TGA in quality control of SWCNTs. **Analytical and Bioanalytical Chemistry** 396: 1071 - 1077.
- Mozurkewich, M. and S.W. Benson. 1984. Negative Activation Energies and Curved Arrhenius Plots. 1. Theory of Reactions over Potential Wells. **The Journal of Physical Chemistry** 88: 6429 – 6435.
- Mohamed, A.N. 2011. Steam Reforming of Methane over Ni/Al₂O₃ Catalysts in a Probe Reactor. **2nd International Conference on Chemical Engineering and Applications. International Proceedings of Chemical, Biological & Environmental Engineering. International Proceedings of Computer Science and Information Technology. Singapore. vol. 23.**

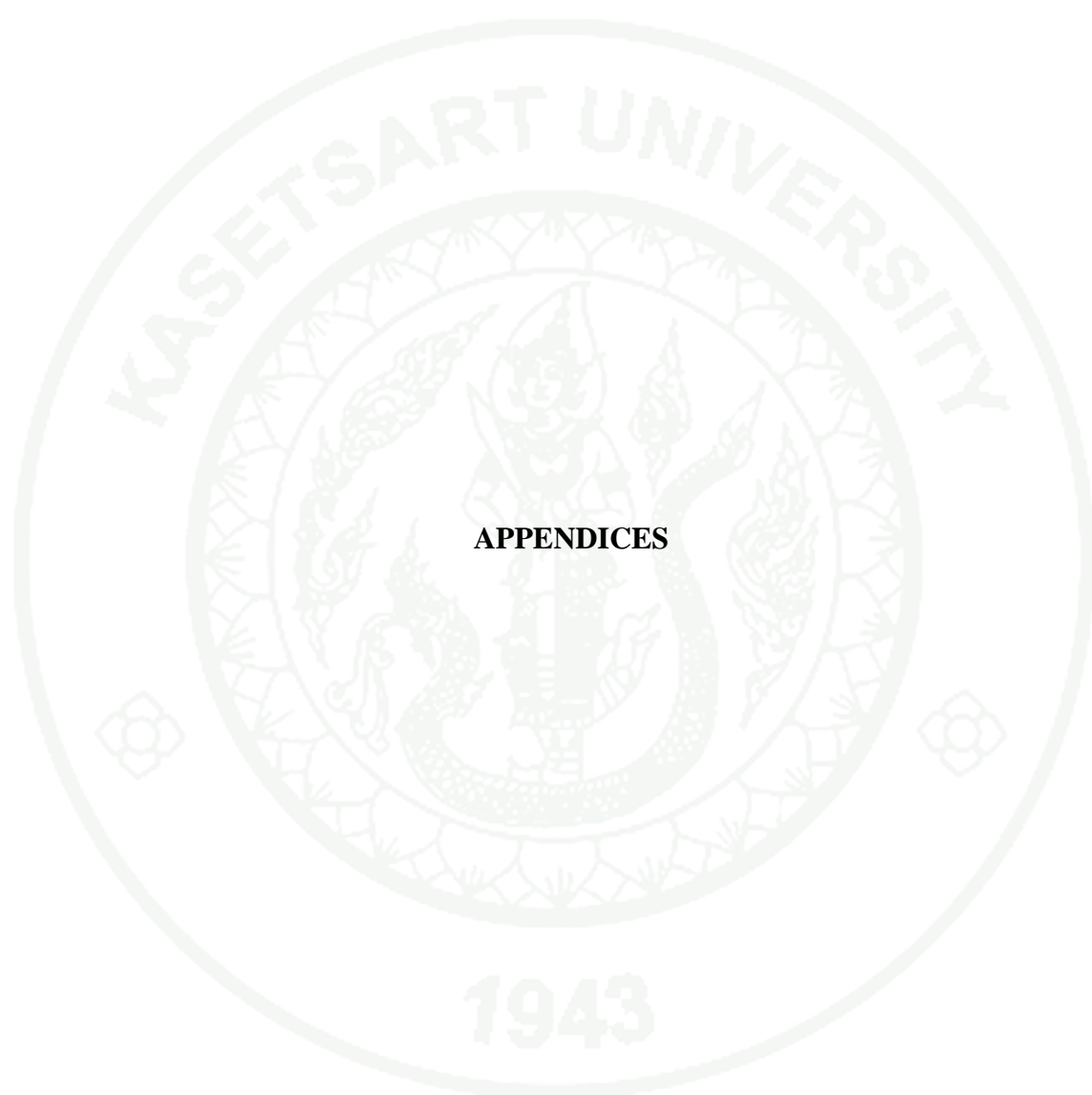
- Moulijn, J.A., P.W.N.M. van Leuwen, R.A. van Santen. 1993. CATALYSIS An integrated Approach to Homogeneous, Heterogeneous and Industrial Catalysis. 79. **Elsevier Science Publishers B.V.**. Netherlands.
- Naito, S. 2000. Methane conversion by various metal, metal oxide and metal carbide catalysts. **Catalysis Surveys from Japan** 4: 3 - 15.
- Niu, Z. and Y. Fang. 2007. Effects of composition of catalysts on the preparation of single-walled carbon nanotubes synthesized over W-Co-MgO catalysts. **Superlattices and Microstructures** 41: 62 - 70.
- Poirier, M.G. and C. Sapundzhiev, 1997. Catalytic decomposition of natural gas to hydrogen for fuel cell applications. **International Journal of Hydrogen Energy** 22: 429 – 433.
- Pompeo, F., D. Gazzoli and N.N. Nichio. 2009. Stability improvements of Ni/ α -Al₂O₃ catalysts to obtain hydrogen from methane reforming. **International Journal of Hydrogen Energy** 34: 2260 - 2268.
- Rahman, M., E. Croiset and R. Hudgins. 2006. Catalytic decomposition of methane for hydrogen production. **Topics in Catalysis** 37: 137 - 145.
- Sharif, H.S.Z., R.M. Abdul and P. SeshaTalpaSai. 2004. Kinetic studies on catalytic decomposition of methane to hydrogen and carbon over Ni/TiO₂ Catalyst. **Industrial & Engineering Chemistry Research** 43: 4864 – 4870.
- Shinoda, M., Y. Zhang, Y. Yoneyama, K. Hasegawa and N. Tsubaki. 2004. New bimodal pore catalysts for Fischer–Tropsch synthesis. **Fuel Processing Technology** 86: 73– 85.

- Snoeck, J.W., G. F. Froment and M. Fowles. 1997. Kinetic study of the carbon filament formation by methane cracking on a nickel catalyst. **Journal of Catalysis** 169: 250 - 262.
- Takahashi, R., S. Sato, S. Tomiyama, T. Ohashi and N. Nakamura. 2007. Pore structure control in Ni/SiO₂ catalysts with both macropores and mesopores. **Microporous and Mesoporous Materials** 98: 107–114.
- Takenaka, S., H. Ogihara, I. Yamanaka, K. Otsuka. 2001. Decomposition of methane over supported-Ni catalysts: effects of the supports on the catalytic lifetime. **Applied Catalysis A - General** 217: 101 - 110.
- Tsoncheva, T., J. Rosenholm, C.V. Teixeira, M. Dimitrov, M. Linden and C. Minchev. 2006. Preparation, characterization and catalytic behavior in methano ldecomposition of nanosized iron oxide particles withinlarge pore ordered mesoporous silicas. **Microporous and Mesoporous Materials** 89: 209–218.
- Venugopal, A., K.S. Naveen, J. Ashok, P.D. Hari, K.V. Durga and K.B.S Prasad. 2007. Hydrogen production by catalytic decomposition of methane over Ni/SiO₂. **International Journal of Hydrogen Energy** 32:1782 - 1788.
- Villacampa, J.I., C. Royo and E. Romeo. 2003. Catalytic decomposition of methane over Ni-Al₂O₃coprecipitated catalysts reaction and regeneration studies. **Applied Catalysis A - General** 252: 363 - 383.
- Vicente, J.L., A. Albesa, J.L. Llanos, E.S. Flores, A.E. Fertitta, D.B. Soria, M.S. Moreno and M. Rafti. 2011. **The Journal of the Argentine Chemical Society** 98: 29 – 38.

Witoon, T., M. Chareonpanich and J. Limtrakul. 2008. Synthesis of bimodal porous silica from rice husk ash via sol–gel process using chitosan as template. **Materials Letters** 62: 1476–1479.

Zhang, T. and M.D. Amiridis. 1998. Hydrogen production via the direct cracking of methane over silica-supported nickel catalysts. **Applied Catalysis A – General** 167: 161 - 172.

Zhang, L., J. Shi, J. Li, Z. Hua, and M. Ruan. 2008. Carbon nanostructures formed on mesoporous silica by catalytic chemical vapor deposition of ethane. **Journal of Materials Research** 23: 435 - 443.



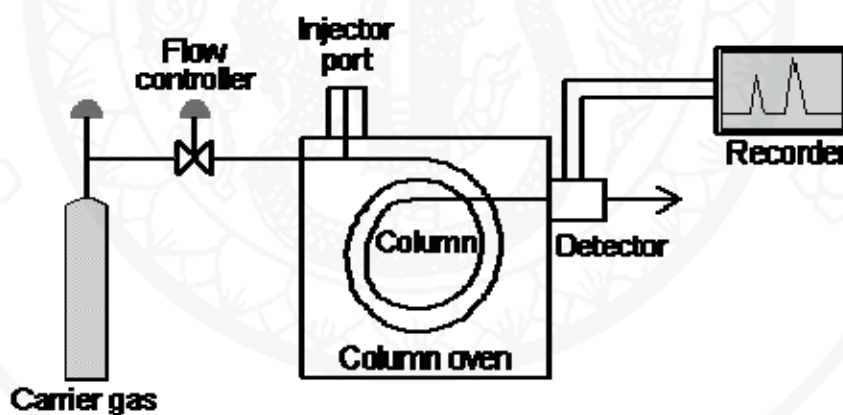
The seal of Kasetsart University is a large, circular emblem in the background. It features a central figure, likely a deity or royal figure, surrounded by a wreath. The outer ring of the seal contains the text "KASETSART UNIVERSITY" at the top and "1943" at the bottom. There are also decorative floral motifs on the sides.

Appendix A

Qualitative and quantitative results from gas chromatography

Quantitative and Qualitative Results from Gas Chromatography

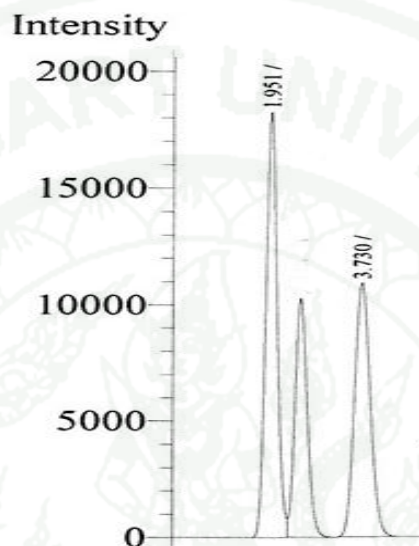
Gas chromatography was performed in a specially designed instrument. The major instrumental components consisted of a flowing mobile phase, an injector port, a separation column containing the stationary phase, a detector, and a data recording system as shown in Appendix Figure A1. Certain amount of gaseous mixture, 0.5 mL in this research, was injected into gas chromatograph at the injector port and was volatilized in a hot injection chamber before it was transported to the head of the chromatographic column. Then, a flow of inert carrier gas (as a mobile phase) swept the injected mixture through a heated column which contained the stationary phase. The gaseous sample moved along the packing column whereas its component gas moved with different flow rates and thus separated into pure component. Before each component exited the instrument, it passed through a detector. The detector sent an electronic signal to the recorder and the analyzed results were printed out.



Appendix Figure A1 Schematic diagram of gas chromatograph.

In this work, the quantitative and qualitative data of product composition was obtained from TCD-GC as mention in the experimental chapter. Before analysis, the condition of operation was set and kept on running for about an hour to stabilize the based line. Certain volume of sample mixture (0.5 mL in this case) was injected into the injection port by gas syringe. After the mixture of sample gas was analyzed, the qualitative and quantitative data were interpreted from the peak area obtained from

the recorder. The component of injected gas mixture can be identified by using the value of retention time data compared with the retention time received from injected standard gas. The chromatogram of standard gases and liquids used in this research were shown as following figures:



Appendix Figure A2 Chromatogram of standard gases for CO and CO₂.

The quantitative analysis of gas and liquid samples were obtained from the calibration curves where the correlation between the amount of injected gas or liquid sample (mole) and the peak area of gas chromatograms were proposed. The correlation between these parameters (mole and area) was analyzed by a linear regression equation. All the calibration curves for each single standard gas and liquid used in this research were shown in Appendix Table A1.

Appendix Table A1 Equation of calibration curves for standard gas and liquid

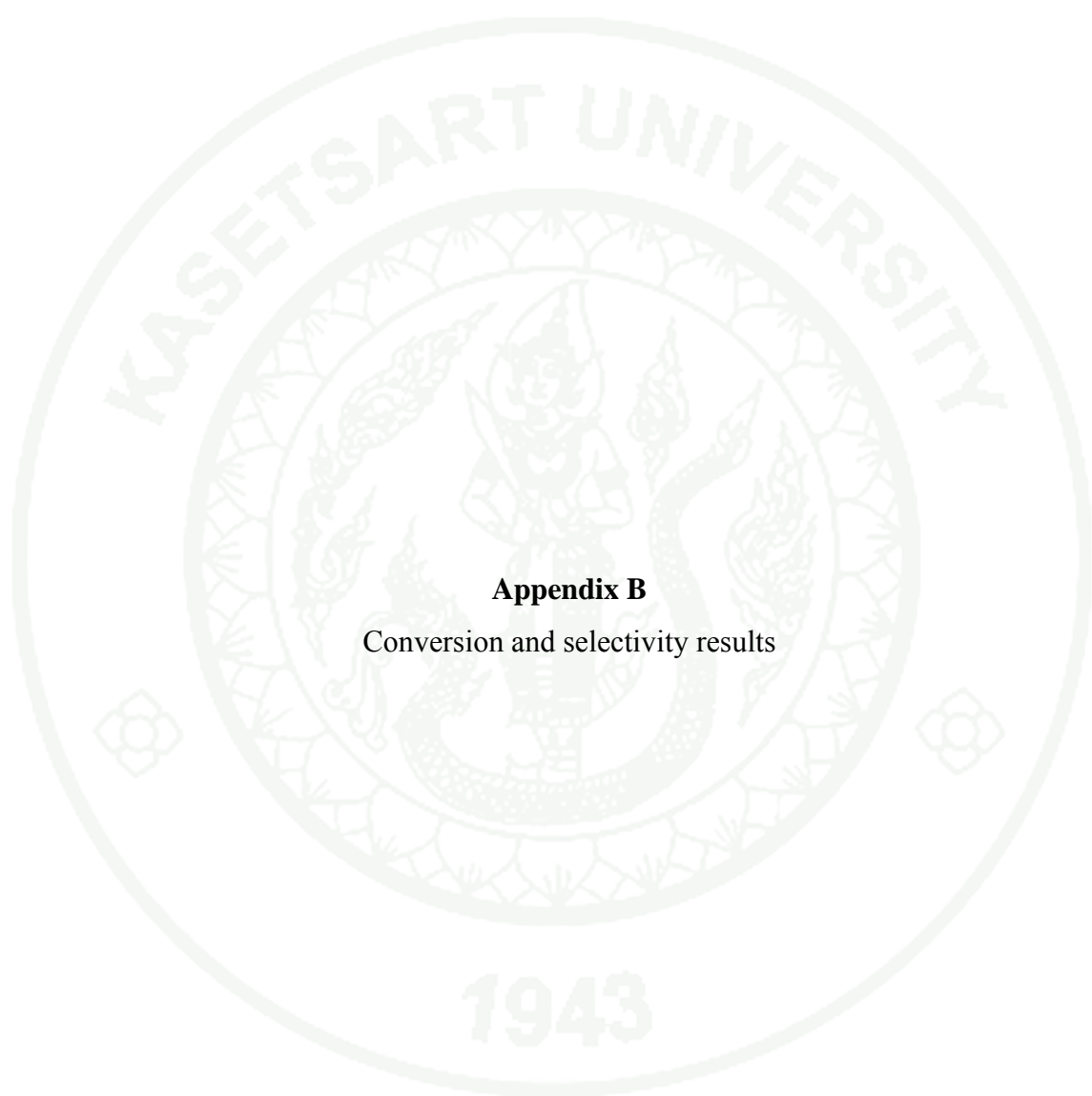
Substance	Equation	R ²
H ₂	mol = 5.0x 10 ⁻¹² x area	0.986
CH ₄	mol = 7.0 x 10 ⁻¹¹ x area	0.999
N ₂	mol = 3.0 x 10 ⁻¹⁰ x area	0.699

The calculation for the amount of each component in a standard-gas mixture can be calculated as follows:

$$\text{Amount of component}_i \text{ (mol)} = \frac{V_i \times T}{100 \times 22,400} \quad (\text{A1})$$

where V_i = % volume of component_i (cm³/cm³)

T = volume of standard gases mixture (mL)



Appendix B

Conversion and selectivity results

Conversion and Selectivity Results

The calculations for the conversion of methane to hydrogen and carbon nanotube in methane cracking reaction are shown as follows:

Percent of CH₄ conversion:

$$\text{CH}_4 \text{ conversion (\%)} = (\text{CH}_{4,\text{in}} - \text{CH}_{4,\text{out}}) / \text{CH}_{4,\text{in}} \times 100$$

Percent of hydrogen yield:

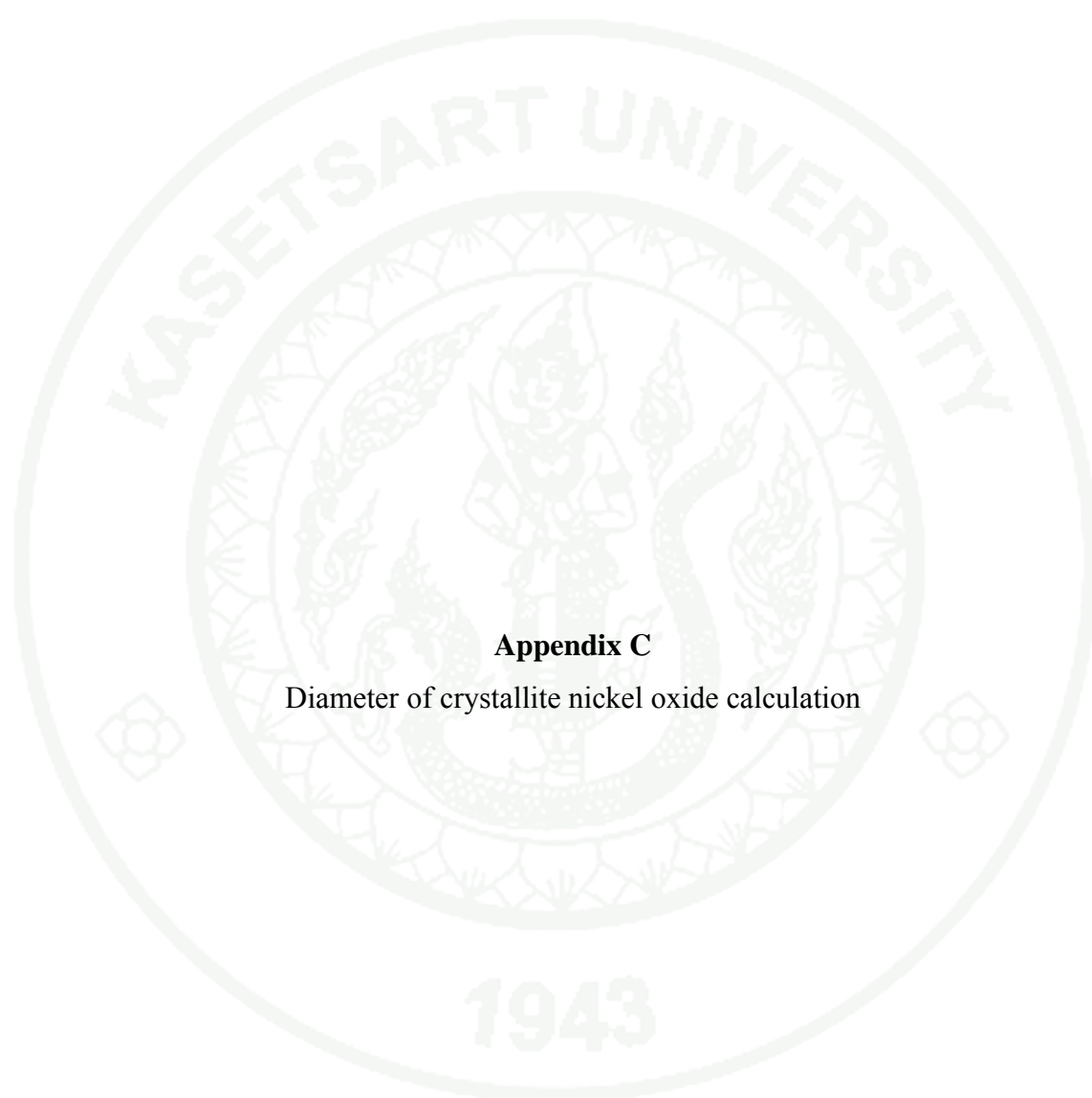
$$\text{Yield of hydrogen (\%)} = \frac{\text{moles of hydrogen} \times 100}{\text{moles of inlet methane}}$$

where CH_{4,in} is a mole number of inlet methane

CH_{4,out} is a mole number of outlet methane

Appendix Table B1 Example of conversion and yield of methane cracking reaction over Ni/BS-2

Description	Calculation
Methane cracking reaction at T = 650°C, P = 1 atm	
Inlet: Peak area of CH ₄	229124.7
CH ₄ mole ($7.0 \times 10^{-11} \times \text{area}$)	1.60×10^{-5} mol
Outlet: Peak area of CH ₄	97710.1
CH ₄ mole	6.84×10^{-6} mol
CH ₄ conversion (%)	57.36
Peak area of H ₂ ($5.0 \times 10^{-12} \times \text{area}$)	835690.5
H ₂ yield (%)	26.05



Appendix C

Diameter of crystallite nickel oxide calculation

Diameter of crystallite nickel oxide calculation

The calculation of crystallite nickel diameter is used Sherer's equation, as shown below:

$$d = \frac{0.89\lambda}{B \cos \theta} \times \frac{180^\circ}{\pi} \quad (C1)$$

where

d is the mean crystallite diameter

λ is the X-ray wave length (1.54 Å)

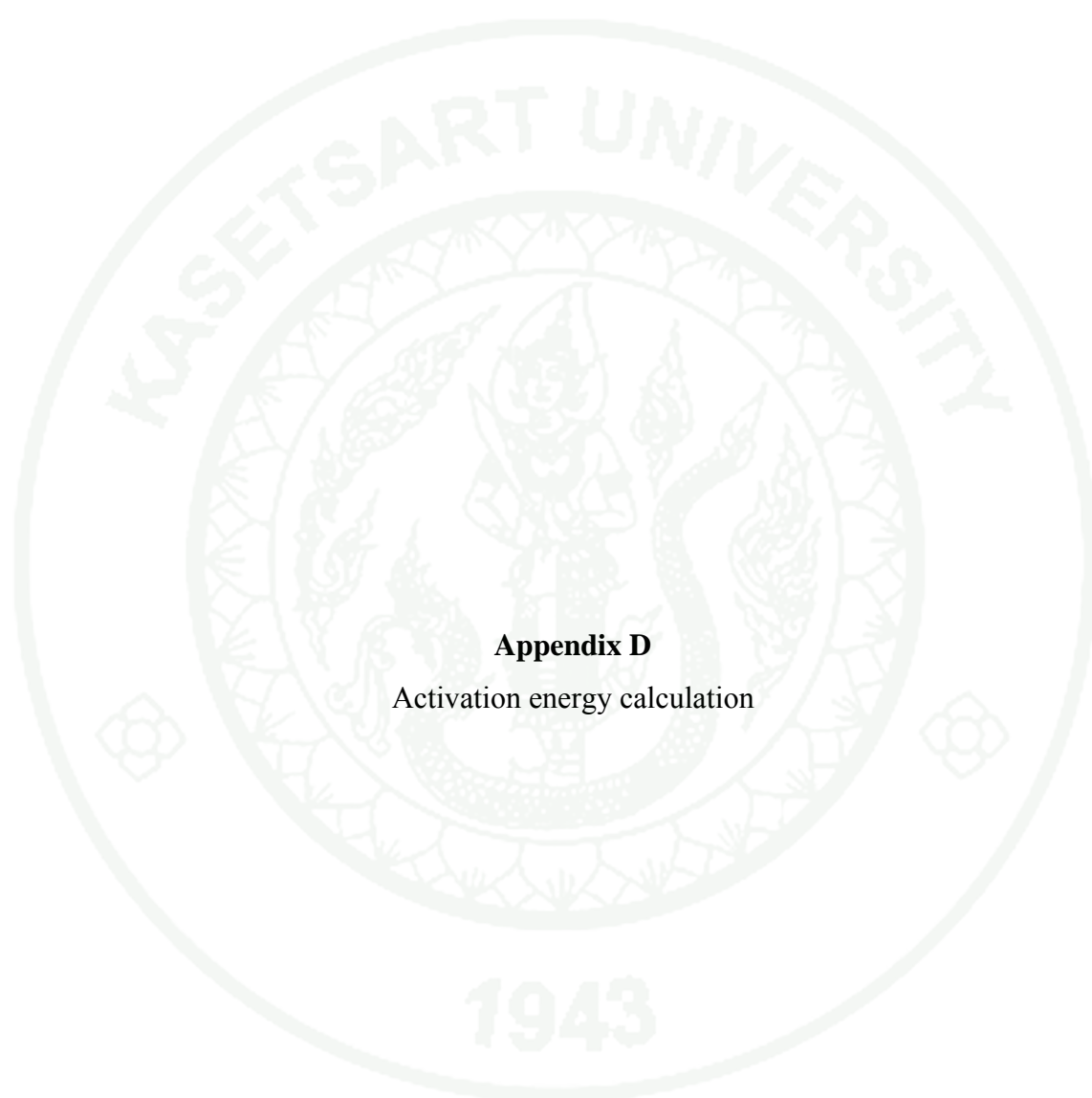
B is the full width half maximum (FWHM) of the NiO diffraction peak.

The example of crystallite NiO diameter of Ni/BS-2 calculation is shown below:

$$B = 0.575^\circ$$

$$d = \frac{0.89 \times 0.154 \text{ (nm)}}{0.575 \times \cos(24.5)} \times \frac{180^\circ}{\pi}$$

$$d = 14.68 \text{ nm}$$



Appendix D

Activation energy calculation

Activation energy calculation

In order to calculate the activation energy, methane cracking reaction is assumed to be 1st order reaction and used an equation shown below:

$$k\tau = (1 + \varepsilon_A) \ln \left(\frac{1}{1 - X_A} \right) - \varepsilon_A X_A \quad (D1)$$

and

$$\varepsilon_A = \frac{V_{X_A=1} - V_{X_A=0}}{V_{X_A=1}} \quad (D2)$$

$$\tau = \frac{C_{A0} V}{F_{A0}}$$

Where ε_A = fractional volume change on complete conversion of A

$$V_{X_A=1} = 2$$

$$V_{X_A=0} = 1$$

X_A = CH₄ conversion

τ = space-time

C_{A0} = mole of A entering / volume of feed

V = volume of reactor

F_{A0} = mole A entering / time

The example of activation energy calculation is Ni/BS-, as shown below:

$$\varepsilon_A = \frac{2-1}{1} = 1$$

And

CH₄ Conversion of Ni/BS-2 at 650°C:

$$X_A = 0.51$$

$$F_{A0} = 1.58 \times 10^{-5} \text{ mol/h}$$

$$\tau = \frac{0.0032077(\text{mol} / \text{L}) \times 0.43 \text{cm}^3}{1.58 \times 10^{-5} \text{mol} / \text{s}} \times \frac{1 \text{L}}{1,000 \text{cm}^3} = 0.87 \text{ s}$$

So $\kappa(0.87) = (1+1) \ln \left(\frac{1}{1-0.51} \right) - (1 \times 0.51)$

$$\kappa = \frac{2 \ln \left(\frac{1}{1-0.51} \right) - 0.51}{0.87}$$

$$\kappa = 1.07$$

Then, the calculations of other operating temperatures are followed the step above and summarized in Table D1.

Table D1 Summarized κ and temperature

T (K)	1/T x 1,000 (K ⁻¹)	κ	ln (κ)
923	1.08	1.07	0.067
873	1.14	0.92	- 0.077
823	1.21	0.57	- 0.563
773	1.29	0.50	- 0.691

The activation energy is calculated from the gradient of Arrhenius's plot, as shown in Figure D1.

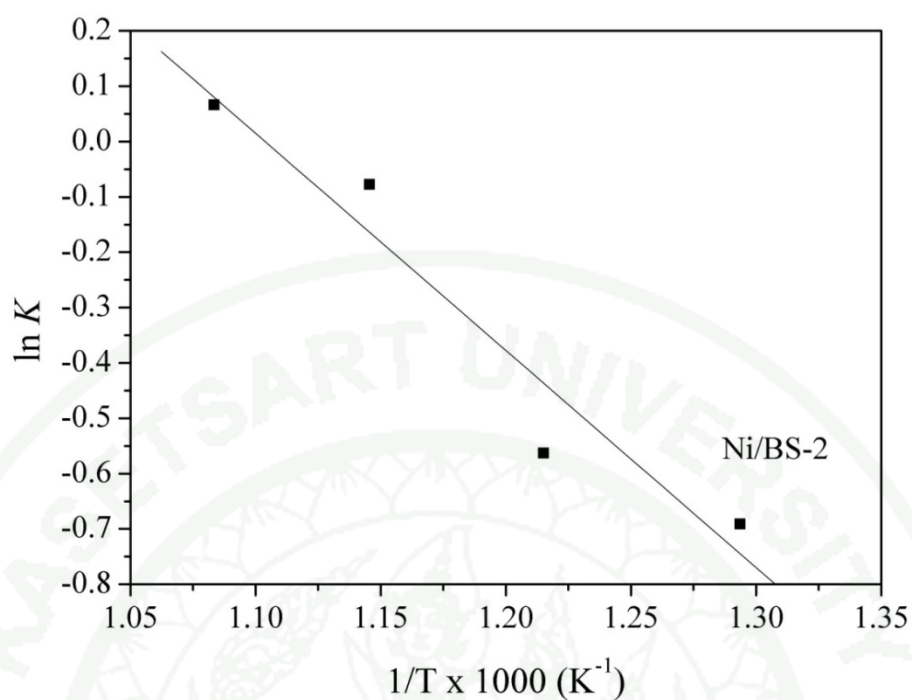


Figure D1 Arrhenius's plot of Ni/BS-2.

The equation of the Arrhenius's plot is $Y = -7.701X + 6.790$

So, the gradient ($-E_a/R$) is -7.701

$$-E_a = -7.701 \times R$$

$$-E_a = -7.701 \times 8.314 \times 1,000$$

$$-E_a = 64.03 \text{ KJ/mol}$$

The activation energies of other catalysts are following the processes above and summarized in Table D2.

Table D2 Summarized activation energies of nickel supported on monomodal and bimodal porous silica supports

Catalysts	Ea (KJ/mol)
Ni/MS-1	-72.0658
Ni/MS-2	-113.569
Ni/BS-1	80.5294
Ni/BS-2	64.02611

CIRRICULUM VITAE

NAME : Mr. Jakkraphun Kitmanacharounpong

BIRTH DATE : September 22, 1986

BIRTH PLACE : Samuthprakarn, Thailand

EDUCATION	: <u>YEAR</u>	<u>INSTITUTE</u>	<u>DEGREE</u>
	2008	Kasetsart Univ.	B.Eng. (Chemical)

SCHOLARSHIP : Teacher Assistant Scholarship from ADB Program of
Department of Chemical Engineering, Kasetsart University
2010-2011